

Air Force Institute of Technology

AFIT Scholar

Theses and Dissertations

Student Graduate Works

3-13-2003

Electrical Activation Studies of Silicon Implanted Al_xGa_{1-x}N and Coimplanted GaN

Elizabeth A. Chitwood

Follow this and additional works at: <https://scholar.afit.edu/etd>



Part of the [Semiconductor and Optical Materials Commons](#)

Recommended Citation

Chitwood, Elizabeth A., "Electrical Activation Studies of Silicon Implanted Al_xGa_{1-x}N and Coimplanted GaN" (2003). *Theses and Dissertations*. 4162.

<https://scholar.afit.edu/etd/4162>

This Thesis is brought to you for free and open access by the Student Graduate Works at AFIT Scholar. It has been accepted for inclusion in Theses and Dissertations by an authorized administrator of AFIT Scholar. For more information, please contact AFIT.ENWL.Repository@us.af.mil.



**ELECTRICAL ACTIVATION STUDIES OF SILICON IMPLANTED $\text{Al}_x\text{Ga}_{1-x}\text{N}$
AND COIMPLANTED GaN**

THESIS

Elizabeth A. Chitwood

AFIT/GAP/ENP/03-01

**DEPARTMENT OF THE AIR FORCE
AIR UNIVERSITY**

AIR FORCE INSTITUTE OF TECHNOLOGY

Wright-Patterson Air Force Base, Ohio

APPROVED FOR PUBLIC RELEASE; DISTRIBUTION UNLIMITED.

The views expressed in this thesis are those of the author and do not reflect the official policy or position of the United States Air Force, Department of Defense, or the U.S. Government.

AFIT/GAP/ENP/03-01

ELECTRICAL ACTIVATION STUDIES OF SILICON IMPLANTED $\text{Al}_x\text{Ga}_{1-x}\text{N}$ AND
COIMPLANTED GaN

THESIS

Presented to the Faculty

Department of Engineering Physics

Graduate School of Engineering and Management

Air Force Institute of Technology

Air University

Air Education and Training Command

In Partial Fulfillment of the Requirements for the

Degree of Master of Science (Applied Physics)

Elizabeth A. Chitwood, BS


March 2003

APPROVED FOR PUBLIC RELEASE; DISTRIBUTION UNLIMITED

ELECTRICAL ACTIVATION STUDIES OF SILICON IMPLANTED $\text{Al}_x\text{Ga}_{1-x}\text{N}$ AND
COIMPLANTED GaN

Elizabeth A. Chitwood, BS

Approved:



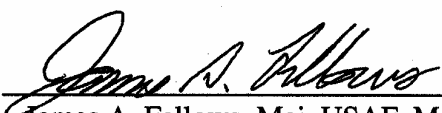
Dr. Yung Kee Yeo, Advisor

12 March '03
date



Dr. Robert L. Hengehold, Member

12 Mar '03
date



James A. Fellows, Maj, USAF, Member

13 MAR 03
date

Acknowledgements

Obtaining a degree for higher education takes the desire of one and the support of many. This project has been no different. I would like to take the time to acknowledge and appreciate the people who aided in the success of this thesis. I would first like to thank my advisor, Dr. Yeo, for his guidance and motivation throughout the project. He provided support when things were tough and his sense of humor when things were stressing. I would also like to extend my gratitude to Greg Smith and Mike Ranft for their technical support. They dedicated long hours to ensure that the equipment was up and running so that my research would not fall behind schedule. I would like to thank Rick Patton for his clean room expertise as well as for his training in clean room techniques. I must also thank Major Jim Fellows for his insight and advice on this research. Dr. Mee Yi Ryu also played a huge role in the understanding and comprehension of the subject matter. She also helped with the sample preparation and data collection. And finally I would like to thank my family and fiancé, for without their support and encouragement I would not be here today. They endure with me the hardships and well as the successes in my drive for higher education. I am forever grateful to the people who have supported and encouraged me as I worked to complete this thesis.

Elizabeth Chitwood

Table of Contents

Acknowledgements.....	iv
List of Figures.....	vii
Abstract.....	ix
1. Introduction.....	1
1.1. Overview.....	1
1.2 High Power Electronics	3
2. Theory.....	5
2.1 Wide Band Gap Semiconductors.....	5
2.1.1 Crystal Structure	5
2.1.2 Semiconductor Basics.....	9
2.1.3 Band Structure	12
2.1.4 Molecular Beam Epitaxy (MBE).....	15
2.2 Ion Implantation and Annealing	17
2.2.1 Ion Implantation.....	17
2.2.2 Coimplantation.....	21
2.2.3 Annealing.....	21
3. Methodology.....	24
3.1 Characterization Method.....	24
3.1.1 Hall Effect Measurements.....	24
3.1.2 Hall Effect Theory	25
3.2 Experimental Procedure.....	29
3.2.1 Sample Growth	29
3.2.2 Sample Preparation for Implantation.....	29
3.2.3 Implantation and Annealing.....	29
3.2.4 Contacts.....	32
3.2.5 Hall Effect Measurements.....	33
4. Results and Discussion	34
4.1 Room Temperature GaN: Si+N	34
4.2 Room Temperature $\text{Al}_x\text{Ga}_{1-x}\text{N}$: Si	41
4.3 Temperature Dependent $\text{Al}_{0.2}\text{Ga}_{0.8}\text{N}$: Si	47
5. Conclusions.....	52

Appendix A.....	55
Bibliography	62
Vita	64

List of Figures

Figure	Page
2.1. The different structures formed by a solid are a) single crystalline, b) polycrystalline and c) amorphous structures.....	6
2.2. More complicated structures formed from the Bravais lattices are the zincblende and wurtzite structures. Examples of theses are a) zincblende GaAs and b) CdS wurtzite structures.....	7
2.3. Band gaps and lattice constants of nitride structures having a) wurtzite and b) zincblende form.	8
2.4. Diagram of the valance and conduction bands for metals, semiconductors, and insulators.	10
2.5. Energy diagram of the acceptor and donor levels forming inside the energy gap region.....	12
2.6. An illustration of a typical Molecular Beam Epitaxy set up.....	16
2.7. An ion implantation depth profile for GaN implanted with silicon ions at various energies.	18
2.8. The design for a typical ion implantation set up.....	19
2.9. An illustration of the radiation damage that can be caused from the implantation of a light ion and a heavy ion.....	20
3.1. A diagram illustration of the van der Pauw Hall effect ¹ showing the forced current, the applied magnetic field, and the accumulation of electrons for an n-type sample.	26
3.2 Layout of the temperature dependant Hall Measurement system.....	28
3.3 Anneal temperature profiles for the different Oxy Gon furnaces located in a) AFRL b) AFIT. Note the time scale difference between the two plots.	31
4.1. Room temperature sheet carrier concentration as a function of anneal temperature for GaN samples coimplanted with various doses and annealed at 1250 and 1300 °C for 29 s.....	35
4.2. Room temperature Hall mobility values for GaN coimplanted with $1 \times 10^{13}/9 \times 10^{12}$, $1 \times 10^{14}/9 \times 10^{13}$, $1 \times 10^{15}/9 \times 10^{14}$ cm ⁻² of silicon and nitrogen, respectively and annealed at 1200 and 1300 °C for 29 s.	37

4.3. The electrical activation efficiency of GaN coimplanted with $1 \times 10^{13}/9 \times 10^{12}$, $1 \times 10^{14}/9 \times 10^{13}$, $1 \times 10^{15}/9 \times 10^{14} \text{ cm}^{-2}$ of silicon and nitrogen, respectively and annealed at 1200 and 1300 °C for 29 s.	38
4.4. Carrier concentration as a function of implanted dose for GaN coimplanted with $1 \times 10^{13}/9 \times 10^{12}$, $1 \times 10^{14}/9 \times 10^{13}$, $1 \times 10^{15}/9 \times 10^{14} \text{ cm}^{-2}$ of silicon and nitrogen, respectively and annealed at 1200 and 1300 °C for 29 s.	40
4.5. Carrier concentrations from room temperature Hall data as a function of anneal temperature for $\text{Al}_x\text{Ga}_{1-x}\text{N}$ implanted with silicon at various doses and annealed from 1200 to 1350 °C. All the samples were annealed for 120 s in AFITs Oxy-Gon furnace, except for the sample indicated by □, which was annealed at AFRL for 29 s.	42
4.6. The mobility values from room temperature Hall data for $\text{Al}_x\text{Ga}_{1-x}\text{N}$ implanted with silicon at various doses and annealed from 1200 to 1350 °C. All the samples were annealed for 120 s in AFITs Oxy-Gon furnace, except for the sample indicated by □, which was annealed at AFRL for 29 s.	44
4.7. The electrical activation efficiencies for $\text{Al}_x\text{Ga}_{1-x}\text{N}$ implanted with doses of 1×10^{14} and $1 \times 10^{15} \text{ cm}^{-2}$ silicon ions and annealed from 1200 to 1350 °C. All the samples were annealed for 120 s in AFITs Oxy-Gon furnace, except for the sample indicated by □, which was annealed at AFRL for 29 s.	46
4.8 The temperature-dependent sheet carrier concentrations taken from 10 – 320 K for $\text{Al}_{0.2}\text{Ga}_{0.8}\text{N}$ implanted with $1 \times 10^{15} \text{ silicon ions/cm}^2$ and annealed at 1250, 1300 and 1350 °C for 120 s.....	48
4.9 The temperature-dependent Hall mobility values taken from 10 – 320 K for $\text{Al}_{0.2}\text{Ga}_{0.8}\text{N}$ implanted with $1 \times 10^{15} \text{ silicon ions/cm}^2$ and annealed at 1250, 1300 and 1350 °C for 120 s.....	49
4.10 The temperature-dependent sheet resistivity data taken from 10 – 320 K for $\text{Al}_{0.2}\text{Ga}_{0.8}\text{N}$ implanted with $1 \times 10^{15} \text{ silicon ions/cm}^2$ and annealed at 1250, 1300 and 1350 °C for 120 s.....	51

Abstract

A comprehensive study of the electrical activation of silicon implanted $\text{Al}_x\text{Ga}_{1-x}\text{N}$ was performed as a function ion dose, anneal temperature, and aluminum mole fraction. Also, GaN coimplanted with silicon and nitrogen was investigated. Room temperature Hall effect measurements were used to determine carrier concentration and mobility. All the samples had a 500 Å encapsulant of AlN, and were implanted at room temperature with 200 keV silicon ions at doses ranging from 1×10^{13} to $1 \times 10^{15} \text{ cm}^{-2}$. The GaN was also implanted with nitrogen under the same conditions in doses of 9×10^{12} to $9 \times 10^{14} \text{ cm}^{-2}$, respectively. The samples were annealed at temperatures ranging from 1200 to 1350 °C for 30 to 120 seconds in a flowing nitrogen environment.

The aluminum mole fractions considered were 0.2 and 0.3. The electrical activation efficiency for the $\text{Al}_{0.2}\text{Ga}_{0.8}\text{N}$ annealed at 1350 °C and implanted with $1 \times 10^{15} \text{ cm}^{-2}$ was almost 90%. While the $\text{Al}_{0.3}\text{Ga}_{0.7}\text{N}$ annealed at 1350 °C and implanted with $1 \times 10^{15} \text{ cm}^{-2}$ exhibited only about 42% activation. The activation efficiency for all the samples increased with anneal temperature, but decreased with aluminum mole fraction. The mobilities and the carrier concentrations demonstrate an increase with the anneal temperature. Although the $\text{Al}_{0.2}\text{Ga}_{0.8}\text{N}$ exhibited almost perfect activation, the mobility was generally low, only $50 \text{ cm}^2/\text{V}\cdot\text{s}$.

The coimplanted GaN showed surprisingly poor results. The highest activation efficiency was only 37% for the sample annealed at 1300 °C and implanted with a dose of $1 \times 10^{15} \text{ silicon ions cm}^{-2}$. The mobilities for these samples were high, on average $100 \text{ cm}^2/\text{V}\cdot\text{s}$. The carrier concentration and activation efficiency were found to increase with implanted dose. The mobilities, however, decreased as the anneal temperature increased.

ELECTRICAL ACTIVATION STUDIES OF SILICON IMPLANTED $\text{Al}_x\text{Ga}_{1-x}\text{N}$ AND COIMPLANTED GaN

1. Introduction

1.1. Overview

The electrical properties of gallium nitride (GaN) and aluminum gallium nitride ($\text{Al}_x\text{Ga}_{1-x}\text{N}$) are investigated as a function of implant dose and anneal temperature. Two mole fractions of $\text{Al}_x\text{Ga}_{1-x}\text{N}$ were studied, 0.2 and 0.3. To characterize their electrical properties, Hall effect measurements were conducted. The objective of this research is to find improved ion implantation conditions and to evaluate the activation efficiencies as a function of anneal temperature. This research seeks greater understanding of how implanted ions affect electrically active centers with the objective of determining the most advantageous implantation and annealing conditions.

The functionality and capabilities of electronics are largely dependent upon the material properties of the semiconductors used to construct them. Silicon remains the most developed semiconductor and over the past fifty years its properties have been largely researched and developed. However, silicon has limitations in high-power, high-temperature, high-frequency electronic ranges, and as such, group III-nitrides are being evaluated as an alternative.

Nitrides possess a wide band gap with high thermal conductivities, high charge carrier velocities, and large breakdown voltages, which allows them to function in extreme temperature and frequency conditions in which silicon fails. Wide band gap semiconductors have been under investigation for a long time due to these promising material properties and they have already been used to produce blue-UV laser diodes, light emitting diodes (LEDs), and UV detectors.¹

Since $\text{Al}_x\text{Ga}_{1-x}\text{N}$ is an alloy of GaN and AlN, it is likely to share many of the same properties and $\text{Al}_x\text{Ga}_{1-x}\text{N}$ should only be slightly more difficult to work with. The high thermal conductivity and stability of the nitrides and their substrates should allow for higher-power laser operation. Lasers based on $\text{Al}_x\text{Ga}_{1-x}\text{N}$ could operate at energies up to 6 eV. Past issues, such as a lack of consistently good substrate material and large n-type background carrier concentration have been resolved using buffer layers on the sapphire and SiC substrates, which have allowed for great improvement in the quality of material grown. The background carrier concentrations have been reduced to $4 \times 10^{16} \text{ cm}^{-3}$ in thin films.²

Yoshida, Misawa, and Gonda³ performed a detailed study of $\text{Al}_x\text{Ga}_{1-x}\text{N}$ and found that the band gap and lattice constant dependencies were linear. They also found that the resistivity of unintentionally doped $\text{Al}_x\text{Ga}_{1-x}\text{N}$ increased rapidly with increasing Al mole fraction with $\text{Al}_x\text{Ga}_{1-x}\text{N}$ becoming insulating above 0.3 aluminum mole fraction. This behavior indicates an increase in impurity ionization energies as the Al mole fraction increases.

1.2 High Power Electronics

Silicon and other elemental semiconductors have been fundamental in the development of microelectronics. However, there are drawbacks. These semiconductors have an indirect band gap, which implies that they emit light very poorly and their absorption coefficients are low. Compound semiconductors, such as group III-nitrides, have many of the desired properties for optoelectronic devices. These devices deal with electronic and optical processes, usually an energy conversion process from electrical to optical or vice versa. Such devices are used in everyday applications such as DVDs, CDs, and notebook computers.

Group III-nitrides have a large energy band gap that enables them to have high thermal conductivities, large breakdown voltages, high saturation velocities, and large cohesion energies. High thermal conductivities allow them to quickly dissipate junction heat, and therefore function more efficiently at high temperature and in high power applications. Wide band gap (WBG) semiconductors also have larger breakdown voltages; the breakdown fields are proportional to the energy gap to the three halves power. This property allows them to be used in high-power amplifiers, switches, and diodes. Smaller devices are also possible due to this characteristic. The internal fields increase linearly as the device dimensions become smaller. WBG semiconductors can also work at high frequencies due to their high saturation velocities. They also have large cohesion energies that make them chemically sound, and less vulnerable in caustic environments as well as more resistant to radiation damage. Additionally, group III-nitrides have direct band gaps (from 1.9-6.2 eV), which is desirable in electrical and optical devices.⁴

The wide band gap nature allows these materials to be used in a wide array of electronic devices. Their ability to withstand high temperatures and caustic environments make them suitable for engine controls and sensors. Nitrides are also used in the fabrication of high-frequency electronic devices. Other applications include devices such as bipolar junction transistors, solar blind photodiodes, and high electron mobility AlGaIn/GaN heterostructures¹⁵. GaN has already been used in the development of electronic devices other than lasers and light emitting diodes. Such devices include heterojunction field effect transistors (HFETs), heterojunction bipolar transistors (HBTs), and high electron mobility transistors (HEMTs).⁵

2. Theory

2.1 Wide Band Gap Semiconductors

Group III - V wide band gap semiconductors crystallize into closely packed structures. The natural growth formation is hexagonal or the wurtzite form for GaN and AlN. The wurtzite nitrides form a continuous system whose direct band gaps range from 3.4 eV in GaN to 6.2 eV for AlN. They can also form zincblende formations. GaN and AlN are well latticed matched, with only a 2.4% difference. The close lattice match allows for greater range and flexibility in heterostructure design.

2.1.1 Crystal Structure

Solids fall into three types of structures:⁶ single crystalline, polycrystalline, and amorphous, which can be seen in Figure 2.1. A single crystalline solid has a well-defined periodic arrangement of atoms throughout the entire crystal. Polycrystalline solids display an ordered arrangement of atoms, in which only the lattice orientation changes in sections of the crystal. If the solid is arranged randomly, it is amorphous. A crystalline structure is a periodic three-dimensional array of atoms held together with electrostatic binding forces.

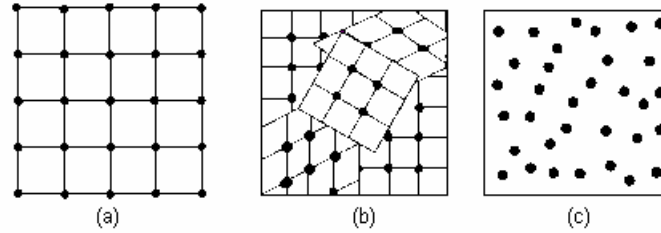


Figure 2.1. The different structures formed by a solid are a) single crystalline, b) polycrystalline and c) amorphous structures.

There are 14 ways of arranging points in space such that the surroundings of each point are identical. These arrangements define 14 unit cells known as Bravais lattices. They can be subdivided into seven crystal systems, each having a unique symmetric property such as invariance under rotational transformation. These groups fully describe the 3-dimensional geometry of the periodic arrays of all crystal solids. Most semiconductors crystallize in the cubic or hexagonal symmetry groups. Structures that are combinations of Bravais lattices are also important. The zincblende structure is comprised of two interpenetrating face-centered cubic Bravais lattices. The wurtzite structure consists of two interpenetrating hexagonal Bravais lattices. Both structures are based on tetrahedral bonding. An illustration of these two structures⁵ can be seen in Figure 2.2.

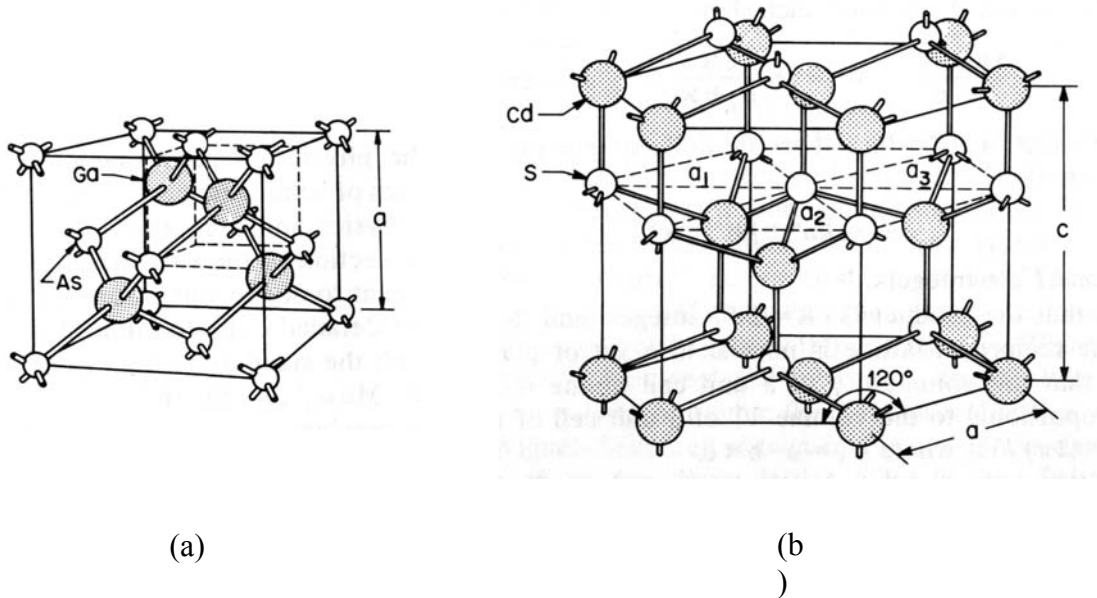


Figure 2.2. More complicated structures formed from the Bravais lattices are the zincblende and wurtzite structures. Examples of these are a) zincblende GaAs and b) CdS wurtzite structures.

Crystalline solids are characterized by their lattice constant, which defines the size of the unit cell. For cubic symmetry, all three dimensions have the same length so that this group can be described by one lattice constant. The hexagonal symmetry group is described by two lattice constants. It is important to closely match the lattice constants of the growth plane and the semiconductor in the growing process. A diagram of the energy gap and lattice constant for group three nitrides⁶ can be seen in Figure 2.3. Note the close match in lattice constant between GaN and AlN.

Crystals do not always have a perfect crystalline structure. There are imperfections such as lattice vacancies and extra interstitial atoms. Point defects include vacancies, interstitials, and antisites. When an atom is missing from a lattice site and the position is left empty, this is called a vacancy. An interstitial is formed when an atom comes to rest

next to a lattice site. If a lattice position is filled with an atom of the wrong subspecies, an antisite is formed. Complex defects are formed from a cluster of point defects. Dislocation lines are complex defects that form in response to a mismatch in the lattice constants of the sample and the growing plane.

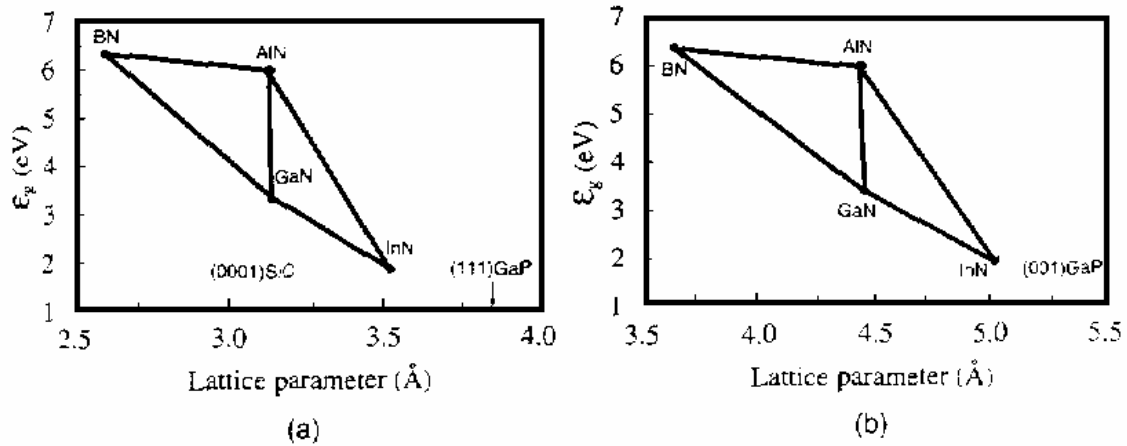


Figure 2.3. Band gaps and lattice constants of nitride structures having a) wurtzite and b) zincblende form.

Strong attractive forces tightly bind the atoms to each other in a periodic formation with only about 2 Å separating the atoms. The atoms are so close together that their electron distributions begin to overlap and interact. The nucleus and core electrons are well bound to their equilibrium position. The valence electrons are free to move in the direction of an applied electric field. Electromagnetic forces are important for maintaining the stability of solids as crystals are held together by a net electrostatic attraction between the positively-charged immobile lattice ions and the gas of negatively-charged electrons. The electrostatic force is governed by Coulomb's inverse square law, which describes the Coulombic attraction between particles.

2.1.2 Semiconductor Basics

Electrons begin to occupy the lowest energy level first and move to higher levels as the number of electrons is increased. Some energy levels are forbidden due to the wavelike properties of the electrons in the material. The allowed energy levels form into bands in solids in response to the overlap in the electron wave functions as a result of the close proximity of the atoms. The highest filled band at a temperature of zero Kelvin (absolute zero) is the valence band. The first unfilled band at this temperature is the conduction band.

Materials are divided into three groups based on their ability to conduct electricity. These groups consist of insulators, conductors and semiconductors. Metals, which are conductors, conduct electricity easily due to an overlap between their valence and conduction bands. When this occurs there are more energy levels available to the electrons than there are electrons to fill them. This allows the electrons to freely participate in the conduction process. Insulators, on the other hand, have a large band gap far greater than the thermal energy of the electron, and electrons fill the valence band completely, and thus do not participate in conduction. Semiconductors have a small energy gap between the valence and conduction bands, and thus electrons can be thermally excited into the conduction band. Band theory of materials is used to explain the differences in these materials. Figure 2.4 is a schematic of the energy bands in conductors, insulators, and semiconductors.

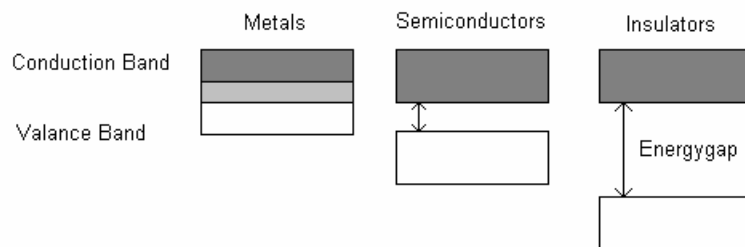


Figure 2.4. Diagram of the valence and conduction bands for metals, semiconductors, and insulators.

An elemental semiconductor consists of atoms of all the same species. These semiconductors are held together by covalent bonds. Compound semiconductors, such as group III-V nitrides, contain two or more elements. The group III-V nitrides get their name because the elements come from the third and fifth columns of the periodic table, respectively, which implies that they have three and five valence electrons. The difference in electronegativity leads to a combination of covalent and ionic bonding. A ternary semiconductor has a small addition of a third element, such as $\text{Al}_x\text{Ga}_{1-x}\text{N}$, where the x denotes the fraction of the different species in the composition.

Intrinsic semiconductors are pure semiconductor materials, which means that they contain no intentional impurity atoms. At room temperature, these semiconductors have a small number of electrons in the conduction band. As the temperature rises, the thermal energy of the electrons increases so that more electrons enter into the conduction band. When an electron moves into the conduction band, it leaves behind a vacancy in the

valence band. This vacancy is referred to as a hole and can be thought of as a second charge carrier with a positive charge. For each free electron in the conduction band, there is a hole in the valence band flowing in the opposite direction. Holes and electrons formed in this way are referred to as intrinsic charge carriers. A variation in the energy gap among III-V nitrides implies that there will be variations in the intrinsic carrier concentrations for different semiconductor materials as a function of temperature.

Intentionally adding impurity atoms to intrinsic semiconductors forms extrinsic semiconductors. The effect of the dopant atom depends on the lattice site it occupies. Atoms from the fourth column of the periodic table can act as acceptors or donors in III-V nitrides, depending on which lattice sites they occupy. Such impurities are called amphoteric.

Transitions that occur from near the bottom of the conduction band to the valence band maximum are normally of interest. At this point, it becomes useful to draw the energy band structure as a function of energy position. In this representation of energy bands, the acceptor and donor levels form in the gap region as shown in Figure 2.5. At absolute zero temperature, carriers from donors and acceptors are bound to their respective atoms and therefore do not contribute to conduction. At non-zero temperatures, sites can become thermally ionized, releasing their carriers into the conduction or valence bands. Donor atoms donate an electron to the conduction band, while acceptors have a hole orbiting around the lattice site.

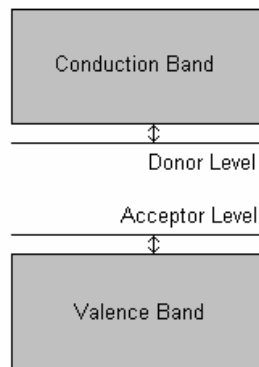


Figure 2.5. Energy diagram of the acceptor and donor levels forming inside the energy gap region.

At low temperature, excitation from donors and acceptors can be the only source for the carriers. Conductivity is extrinsic at this point. At high temperatures, there is direct thermal excitation from the valence band to the conduction band, making the conductivity intrinsic.

2.1.3 Band Structure

From quantum mechanics, it is known that electrons have discrete allowable energy values in solids. When a solid is formed the atoms are very close together, about two angstroms apart. The electrons that are close to the nucleus are very tightly bound to the nucleus through electromagnetic forces. These electrons shield the outer, valance electrons from the positive attraction of the nucleus. The valence electrons can then be considered free particles loosely bound to the inner ion. The positive ion core sits at the lattice site positions, and the outer electrons swarm around them. In the solid, the atoms are in such close proximity that the electron wave functions overlap and the electrons

form a cloud. The electrons are thus free to move around the solid. The discrete energy levels of the electrons merge together in this instance to form energy bands.

A band structure diagram is an illustration of the change in energy with the wave vector, k . The most important bands to consider are the valence and conduction bands. If both the valence band maximum and the conduction band minimum occur at a value of the effective crystal momentum equal to zero or at $k = 0$, then the semiconductor is said to have a direct band gap. Semiconductors in which the bottom of the conduction band occurs at other points in momentum space are indirect materials. The valence and conduction bands are best approximated by parabolic functions of k in this region. For the conduction band the energy is given by

$$E_c = E_g + \hbar^2 k^2 / (2 m_e^*), \quad (1)$$

where m_e^* is an electron effective mass, E_g is the energy gap and \hbar is Planck's constant reduced. The corresponding energy equation for the valence band is

$$E_v = - \hbar^2 k^2 / (2 m_h^*), \quad (2)$$

where m_h^* is a hole effective mass. The reference energy level is the top of the valence band. Electrons are fermions and as such they are governed by the Fermi-Dirac distribution.

$$f(E) = \frac{1}{\exp\left[\frac{E - E_F}{k_B T}\right] + 1} . \quad (3)$$

Here, E_F is the Fermi energy, T is the temperature and k_B is the Boltzman constant. The Fermi energy is the energy at which there is a fifty percent chance of finding an electron at this energy. The densities of states for the valance and conduction bands are given by equation 4. The energy, E , is measured from the bottom of the conduction band.

$$g_{c,v}(E) = \frac{\sqrt{2|(E - E_{c,v})|}}{\pi^2 \hbar^3} (m_{e,h}^*)^{3/2} . \quad (4)$$

The effective mass, $m_{e,h}^*$, is determined by considering the dynamics of the wave-packet of a localized particle. The wave-packet moves with a group velocity given by

$$v_g = \frac{dw}{dk} = \frac{1}{\hbar} \frac{dE}{dk} . \quad (5)$$

The effective masses are found through the following relations

$$m_e^* = \frac{\hbar^2}{d^2 E_c / dk^2} \quad \text{and} \quad m_h^* = \frac{\hbar^2}{d^2 E_v / dk^2} . \quad (6)$$

When an electron enters the conduction band, it leaves behind a hole in the valence band, which allows for free hole conduction. Semiconductors have positive and negative charge

carriers at the same time. The total conductivity of the material is the sum of the conductivity from both charge carriers. This allows for controlled modulation of the conductivity and other material properties. The conductivity (σ) and mobility (μ) are related through the following equation.

$$\sigma = e(n\mu_n + p\mu_p). \quad (7)$$

Where n and p are the concentrations of electrons and holes in the conduction and valence band, respectively, μ_n and μ_p are the electron and hole mobility and e is the charge of the carriers. The hydrogen atom can be used to approximate the ionization energy of the impurity species.⁵ For the hydrogen atom this energy is given by

$$E = -\frac{m_0 e^4}{2\hbar^2 \kappa^2} = -13.06 \text{ eV}, \quad (8)$$

where κ is $4\pi\epsilon_0$ and ϵ_0 is the permittivity of free space. The energy required to ionize these carriers is much less than the binding energy of the hydrogen atom.

2.1.4 Molecular Beam Epitaxy (MBE)

The samples in this study were grown using molecular beam epitaxy (MBE). This process utilizes surface kinetics and takes place under non-equilibrium conditions. It is a controlled thermal evaporation process that takes place under high vacuum conditions and results in excellent control over growth parameters. Figure 2.6 is an illustration of a typical MBE growth system.⁷

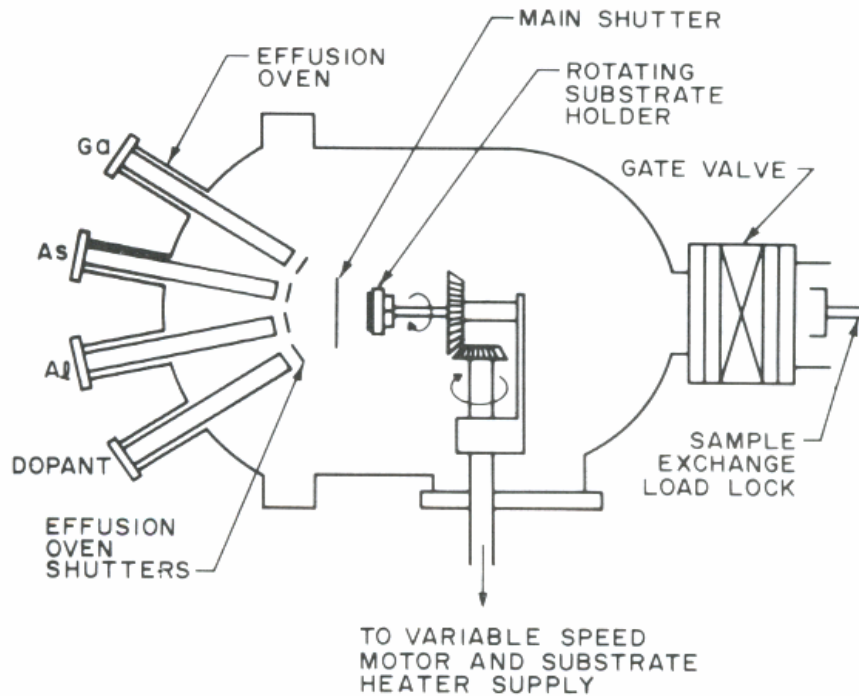


Figure 2.6. An illustration of a typical Molecular Beam Epitaxy set up.

There are three vacuum sections, and of these, the growth chamber is the most important. The load lock is used to transfer the samples to and from the growth chamber without breaking vacuum. Along with the vacuum system, cryopanel are used to help keep the partial pressure down to 10^{-11} Torr. The samples are placed onto a rotational magnetic holder known as a Continual Azimuthal Rotation (CAR). The source atoms are heated until they are able to escape via thermionic emission. Collisions are infrequent, so that the atoms experience a long mean free path in the vacuum chamber. The atoms travel in a straight line until they collide with the substrate material. The shutters control the emission of the different species. The normal growth rate is 10 monolayers per minute, allowing for abrupt changes in the material composition.

To calculate the growth rate, electrons are emitted from an electron gun at a glancing incidence to the substrate holder. The material begins to grow by forming little islands on the substrate. As more material is deposited these islands join together to form flat surfaces. By monitoring the rate of the reflectivity of the electrons, the rate of growth can be determined.

2.2 Ion Implantation and Annealing

The semiconductor is doped to aid in control of material conductivity. This is achieved through doping, whereby the impurity ions change the properties of the semiconductor. The impurities, when introduced in small amounts, act as acceptors or donors depending on the lattice sites they occupy. The main disadvantage to ion implantation is that radiation damage occurs to the crystal structure, which results in the need to anneal the samples at high temperatures.

2.2.1 Ion Implantation

Ion implantation was chosen over in-situ doping during material growth for many reasons. In-situ doping is too time consuming and therefore expensive. Ion implantation also allows for selective area doping as well as control over the doping level. Doping profiles are more easily obtained with ion implantation than with other techniques. The method of implantation also provides good uniformity and sample reproducibility. The major setback is the need to anneal out the crystalline damage caused by the implanted ions. A typical depth profile⁵ can be seen in Figure 2.7. The profile is for the depth of silicon and argon ions at various energies into GaN.

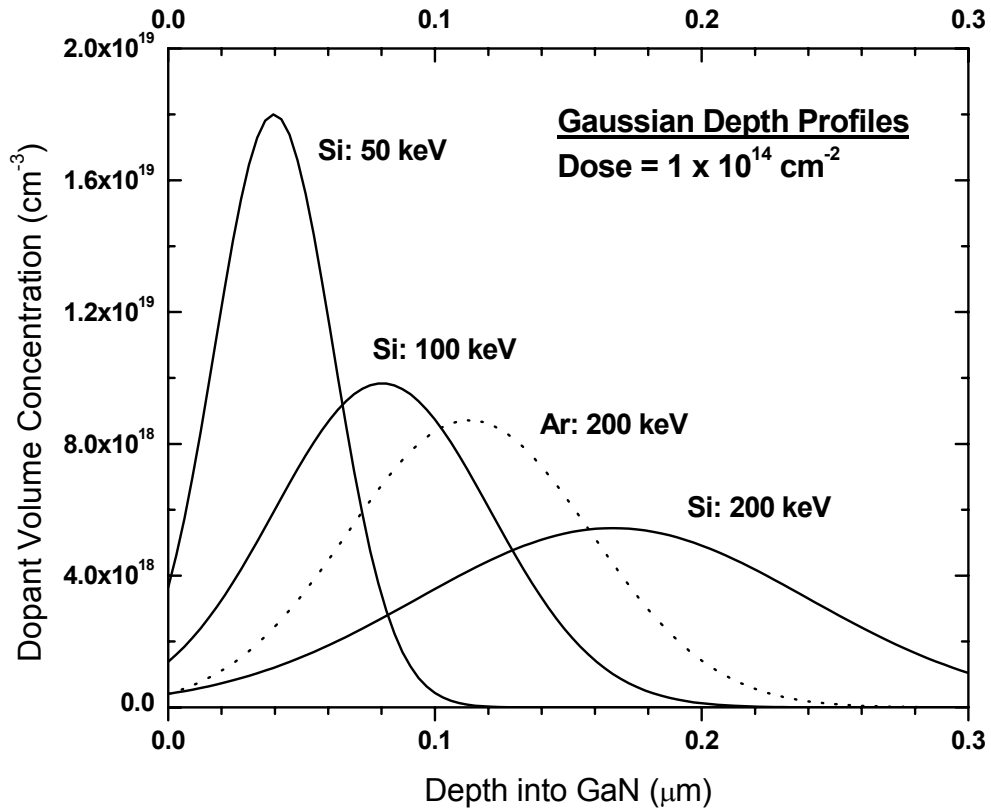


Figure 2.7. An ion implantation depth profile for GaN implanted with silicon ions at various energies.

An ion-implanter⁵ has the following design features: a source chamber, accelerator, mass separator, and target chamber as seen in Figure 2.8. The particles are accelerated down a channel at various energies. The angle of incidence is precisely aligned so that the energy and collision with the host lattice will determine the projected range of the ions. This allows for accurate depth profile charts. The depth profile of the implanted ions has the shape of a Gaussian function. The more intense the energy, the deeper the ions will penetrate into the semiconductor material.

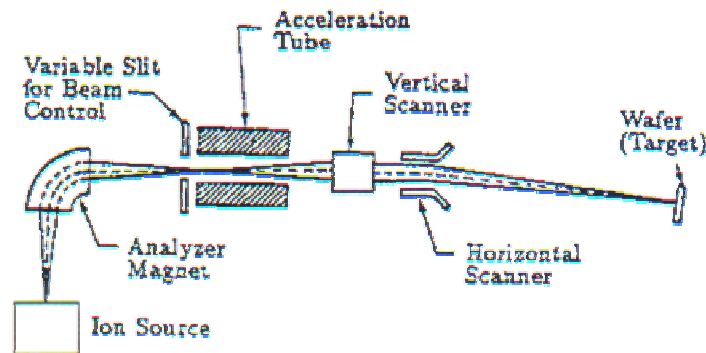


Figure 2.8. The design for a typical ion implantation set up.

The high-energy bombardment of ions leaves the semiconductor material with radiation damage as the incoming ions collide with host atoms. These collisions can cause the host atom to dislodge from its equilibrium position and begin a chain reaction producing a network of defects. The extent of damage done to the host material is determined by the mass of the implanted ion as well as its energy and the dose. The temperature of the substrate during implantation and the atomic mass of the host atoms relative to the implanted ion's mass are also factors. The ionic nature of a material can aid in resisting radiation damage. Group III-nitrides are ionic materials. A diagram of this effect⁵ can be seen in Figure 2.9. Radiation damage has adverse side effects on the electrical properties of the semiconductor material.

Defects can be simple point defects. Examples of these are vacancies, interstitials, and antisites. Antisites occur when host atoms become displaced and come to rest on opposite

lattice positions. Point defects occur when host atoms are removed from equilibrium positions within the crystal lattice. This means there will be unpaired valance electrons that when ionized will make these defects singly or multiply ionized. Implanted ions also form interstitials. A complex is a combination of point defects.

Extended defects are dislocation lines formed by the clustering of simple and complex defects. These defects are also caused in the sample from lattice mismatches between the substrate and semiconductor material. When the displacement concentration becomes equal to the atomic density of the material, amorphization begins.

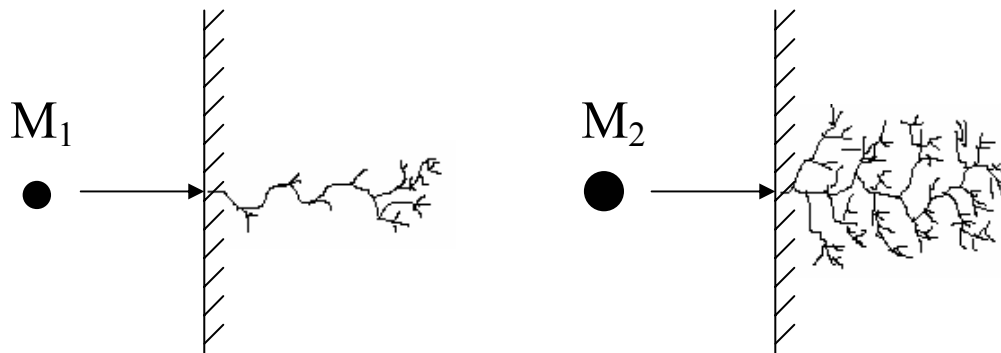


Figure 2.9. An illustration of the radiation damage that can be caused from the implantation of a light ion and a heavy ion.

Defects due to radiation damage can cause the crystal structure to be lost and possibly even become amorphous. To restore crystal structure and activate the implanted ions, the sample must be annealed at a high temperature.

2.2.2 Coimplantation

Coimplantation is thought to help improve stoichiometry of the crystal, and thus the electrical activation by providing a secondary species to fill the sublattice positions of the cation (III) sites. This leaves only the anion (V) site for the primary implant species when creating n-type material. The theory is that the activation of the implanted dopant will increase if stoichiometry is maintained during the implantation process. This would entail implanting the sample with a second dose of the opposite sublattice host atom, in this case nitrogen. The heavier ion is implanted first to create vacancies and other damage that can be filled with the second lighter implanted ion. If the dopant is amphoteric, the coimplant increases the probability that the implant will occupy the desired lattice position.⁵ For this study, GaN was coimplanted with silicon and nitrogen.

2.2.3 Annealing

The annealing process accomplishes two critical tasks: it restores crystal order and it electrically activates the implanted ions. It is a thermodynamic process, allowing a trade-off of temperature and time attributes to yield the optimum results. This research used a rapid thermal anneal (RTA) and conventional furnace anneal (CFAs) with and without a rapid cool-down process.

The rapid thermal anneal is characterized by fast ramp rates (>50 °C/s) and short dwell times (<60 s). RTA utilizes high power quartz halogen lights for a heat source. The short anneal time facilitates production applications. The RTA's short anneal times are also advantageous because many common dopants diffuse quickly into the III-V materials and

alter their implantation profiles. CFAs have much longer ramp rates and anneal times, and can reach and maintain higher temperatures for long periods without reliability concerns.

When ion implanting a sample, it is important to take precautions to avoid amorphization. The mass difference of the group III-V compound's atoms means that the lighter atoms will most likely be further displaced than the heavier ones. With group III-nitrides, anion and cation sublattice positions have to be restored. This process can be more difficult than when dealing with elemental semiconductor materials. Steps also need to be taken to avoid dissociation of the group V atoms during the anneal process. This is a significant concern for nitrogen at the high temperature anneals used in this study.

Precautionary measures can be taken to prevent dissociation. An epitaxially-grown encapsulant can be grown either during or after the initial growth stages. The encapsulant works to prevent out diffusion of implant species and must have high thermal integrity to survive the anneal. It must not react chemically with the implanted layer, and should be easily removed after the anneal. A second precautionary step is to have group V overpressure in the anneal chamber. And finally, a proximity cap anneal can be performed, in which the samples are placed face-to-face during the anneal process.

To determine the most advantageous anneal temperature and time, two types of anneals can be performed: isochronal and isothermal. In isochronal anneals, the anneal time is held constant while the temperature is varied. These can be done in a RTA or a CFA.

With isothermal anneals, in which the time is varied and the temperature is held constant, CFA is the best choice. In general, an anneal temperature of two-thirds of the sample's melting point is required to remove the defect damage caused by implantation.⁵

3. Methodology

3.1 Characterization Method

3.1.1 Hall Effect Measurements

The Hall effect and sheet resistivity measurements were conducted using the standard van der Pauw technique. This technique is convenient because the calculations do not depend on the shape of the sample, only that it be simply connected. The van der Pauw technique also requires that the contacts be on the border of the sample. The sheet resistivity, ρ_s , and the Hall coefficient, R_H , were measured. These two factors allow for the calculation of the sheet carrier concentration, N_s , and Hall mobility, μ_H , through the following relations:

$$N_s = r / (q R_H) \quad \text{and} \quad \mu_H = R_H / \rho_s . \quad (9)$$

Here, q is the electronic charge and r is the ratio of the Hall to drift mobility. The value of r is normally taken to be unity. Hall Measurements provide only an average carrier concentration and mobility values over the entire conducting thickness. A total of 8 current-voltage pair measurements are averaged to calculate the sheet resistivity. Four current-voltage pair measurements averaged under forward and reverse **B** field are averaged to calculate the Hall coefficient. The Hall measurements are also used to determine the activation efficiencies of the implanted samples. The following relation is used:

$$A = \frac{N_s}{D} , \quad (10)$$

where A is the activation efficiency, N_s is the sheet electron concentration, D is the implanted ion dose

From these relations, it can be seen that as the temperature rises, more impurities become ionized causing the carrier concentration and mobility to change. For wide band gap semiconductors, the energy levels are deeper and thus require higher temperatures to activate these levels.

3.1.2 Hall Effect Theory

The sample is placed in a magnetic field such that the sample surface is orthogonal to the field. A current is applied across the sample that induces an electric field. The free charge carriers become subject to the Lorentz Force, which is felt perpendicular to both the **E** and **B** fields.

$$\mathbf{F} = e (\mathbf{v} \times \mathbf{B}). \quad (11)$$

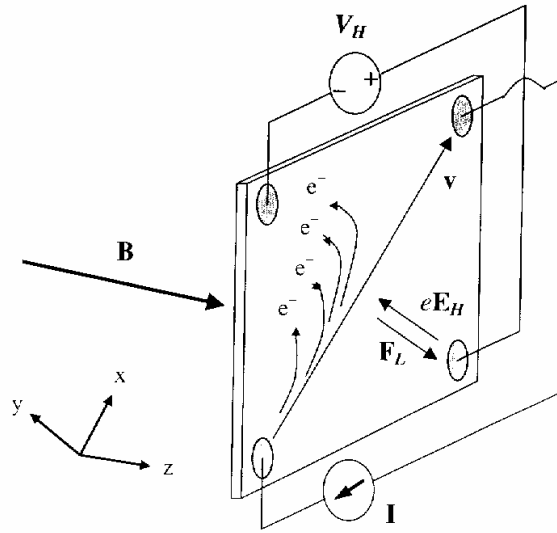


Figure 3.1. A diagram illustration of the van der Pauw Hall effect showing the forced current, the applied magnetic field, and the accumulation of electrons for an n-type sample.

From Figure 3.1⁵ it can be seen that the electrons will move in the y direction in response to the Lorentz Force. The electron and the holes move in opposite directions because they are oppositely charged. The dominant carriers then build up on one side of the sample inducing a Hall voltage in the y direction. The system comes to equilibrium when the force from the Hall voltage is equal to that of the Lorentz force. The magnitude of the Hall voltage is inversely proportional to the carrier concentration and the sign of this voltage indicates the dominant carrier type. The Hall voltage is governed by the following equation

$$V_H = R_{Hs} I_x B_z r. \quad (12)$$

Here R_{Hs} is the sheet Hall coefficient, I_x is the applied current, B_z is the applied magnetic field and r is the ratio of the Hall to drift mobility. The Hall coefficient is given by

$$R_H = t \cdot R_{Hs} , \quad (13)$$

where t is the thickness of the semiconductor layer and R_{Hs} is the sheet Hall coefficient. Determining the Hall coefficient allows for calculation of the carrier concentration and mobility of the sample.

Temperature Dependent Hall (TDH) measurements provide carrier concentrations and mobility values as a function of temperature. At low temperatures, the shallow donor and acceptor impurities should freeze, leaving the material resistive. If the material is highly degenerate, TDH measurements will reveal this degenerate layer at low temperatures via the mobility and carrier concentration will be temperature independent. The samples are placed in a vacuum during the TDH measurements to prevent condensation or oxidation, which would be damaging to the sample and adversely affect measurement accuracy.

Figure 3.2 is a diagram of the TDH configuration⁵ used for these experiments.

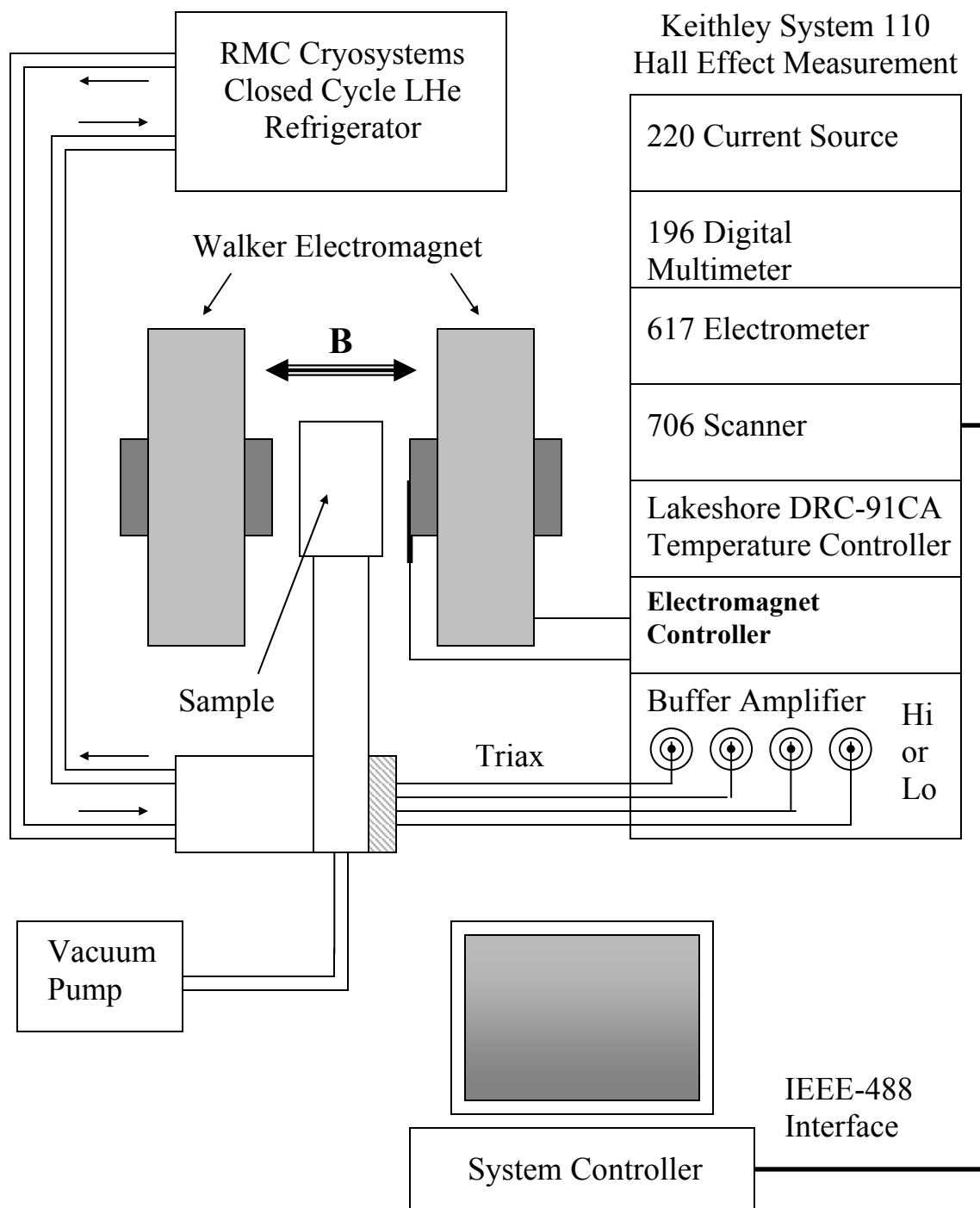


Figure 3.2. Layout of the temperature dependent Hall measurement system.

3.2 Experimental Procedure

3.2.1 Sample Growth

Samples of $\text{Al}_x\text{Ga}_{1-x}\text{N}$ and GaN were purchased from SVT Technologies. Two microns of $\text{Al}_x\text{Ga}_{1-x}\text{N}$ and GaN encapsulated with 500 Å of AlN were grown via MBE using ammonia for a nitrogen source. The samples were grown on two inch sapphire substrates with a 200 Å buffer layer of AlN. The AlN is a better lattice match than the sapphire for both $\text{Al}_x\text{Ga}_{1-x}\text{N}$ and GaN. The better lattice match minimizes defects. The nitride material is grown in 1 to 2- μm thick layers at a growth rate of 1 μm per hour. The backside of the substrate was coated with titanium so that the sample would heat up evenly during the growth process.

3.2.2 Sample Preparation for Implantation

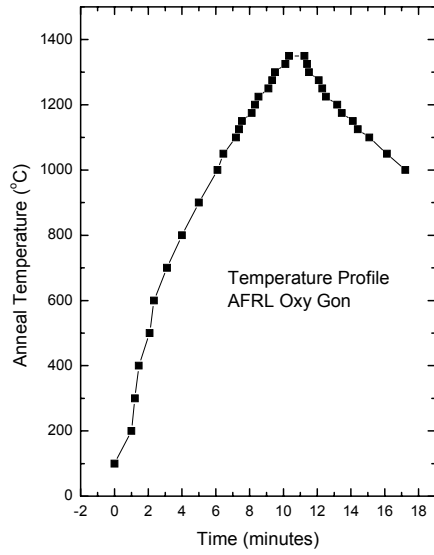
To prepare the samples for implantation, their quality was confirmed via cathodoluminescence measurements. The Ti was removed from the samples with a hydrofluoric acid bath. Then the samples were cut into four quadrants using a diamond-cutting saw. Photoresist 1812 was applied to the samples to protect them during the cutting process. Three of the quadrants were sent to Implant Sciences Corporation for implantation and one quadrant was kept as the control sample. Complete sample preparation procedure can be found in appendix A.

3.2.3 Implantation and Annealing

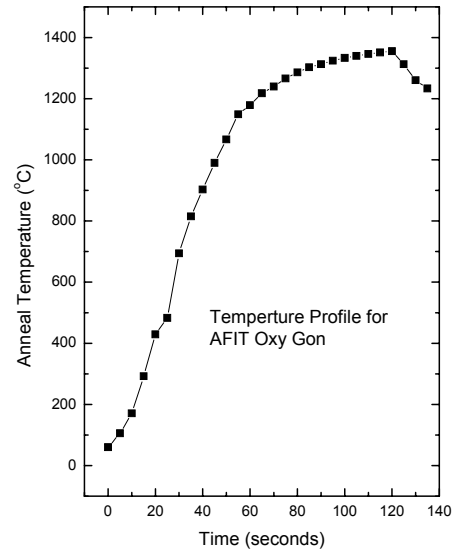
Samples of $\text{Al}_x\text{Ga}_{1-x}\text{N}$ and GaN were implanted at doses ranging from 1×10^{13} to 1×10^{15} cm^{-2} at room temperature with 200 keV silicon ions. The GaN samples were coimplanted

with nitrogen at doses of 9×10^{12} to $9 \times 10^{14} \text{ cm}^{-2}$, respectively. To prepare for the anneal, the samples were cleaned with acetone, methanol, and distilled water, then blow dried with N_2 and coated with photoresist. The samples were then cut into 5 mm by 5 mm squares. The samples were cleaned again and scribed on the backside with a unique symbol to enable identification. The samples were then paired up and wrapped with Ta wire for a proximity cap anneal. The anneal was conducted with an Oxy Gon furnace at the Materials and Manufacturing Directorate located in AFRL, or the one in the AFIT research laboratories.

The AFRL furnace has one chamber that is heated to the desired temperature with the sample placed inside. The process of heating and then cooling the chamber back to room temperature can take upwards of three hours. Figure 3.3a, temperature profile of an anneal performed at 1350°C with the AFRL furnace, shows that the sample spends over 5 minutes above temperatures of 1200°C . The samples are brought up to the anneal temperature for only a short amount of time ($< 30 \text{ s}$) and then the temperature is ramped back down.



(a)



(b)

Figure 3.3 Anneal temperature profiles for the different Oxy Gon furnaces located in a) AFRL and b) AFIT. Note the time scale difference between the two plots.

The AFIT Oxy Gon furnace has two chambers. The first chamber is heated to the desired temperature and the other is used as a load chamber for the samples. The samples are loaded into the second chamber so that they can be inserted into the hot oven and then quickly removed to rapidly cool down to room temperature. The time for these anneals was longer (120 s), but the sample spends less time, only about one minute above 1200 °C, which can be seen in Figure 3.3b. The samples are kept in the sample chamber until they are cooled to room temperature to avoid oxidation of the AlN cap layer. If this layer becomes oxidized, it will be very difficult to remove.

To avoid oxidation, the anneal takes place in a nitrogen rich environment filling up with high purity nitrogen gas after pumping into high vacuum. The samples were annealed for 29 to 120 seconds at temperatures ranging from 1200 to 1350 °C.

3.2.4 Contacts

The Ta wire is brittle and easily removed after the anneal. The samples were placed in a 0.5 molar bath of KOH and distilled water at 95 °C for five minutes to remove the AlN encapsulant. The samples were then rinsed with distilled water and placed in a beaker of aqua regia for two minutes. Next, they were then rinsed again with distilled water and blown dry with nitrogen gas. Finally, they were mounted on a van der Pauw shadow mask in preparation for the deposition of the contact metals. An electron beam evaporator was used for the deposition of the ohmic contact metals. A four layer contact was created by depositing 300 Å of titanium followed by 800 Å of aluminum then 1200 Å of titanium and finally 550 Å of gold for the $\text{Al}_x\text{Ga}_{1-x}\text{N}$ samples. A two-layer contact of 400 Å of titanium and 1200 Å of aluminum was used on the n-type GaN samples. To help the contact metals diffuse into the semiconductor material, the samples were rapid thermal annealed (RTA) in a nitrogen rich environment at 700 °C for 90 seconds for the $\text{Al}_x\text{Ga}_{1-x}\text{N}$ samples and 900 °C for 30 seconds for the GaN samples.

To check the quality of the contacts, a probe station in AFIT's research laboratories was utilized. A small current was sent through the sample and the voltage was measured. If the contacts are ohmic, i.e., follow Ohm's law and the relationship between the current

and the voltage is linear, then Hall measurements can be conducted. Contacts can also be rectifying or simply not pass any current.

The samples with contacts that were found to be rectifying were RTA'd again at 900 °C for 30 seconds. Contacts that exhibited no relation between current and voltage and those that remained rectifying after the second RTA had to have their contact re-deposited. Electrical activation measurements cannot be made if the contacts are not highly ohmic.

3.2.5 Hall Effect Measurements

The Hall measurements were done using a Kiethly 110 system at a temperature range from 10 to 320 K. This low temperature system required gold wires to make a connection to the contacts. The samples were mounted in a closed dewar and placed in vacuum conditions to avoid condensation or oxidation that could alter the accuracy of the measurements. The magnetic field setting was 5 kGauss. The current setting depended on the resistivity of the sample, but ranged from 1 μ A to 1 mA.

Room temperature Hall measurements were taken for both the GaN and the $\text{Al}_x\text{Ga}_{1-x}\text{N}$ samples for all of the different anneal temperatures. TDH data was collected for $\text{Al}_{0.2}\text{Ga}_{0.8}\text{N}$ samples for three different anneal temperatures.

4. Results and Discussion

4.1 Room Temperature GaN: Si+N

The GaN samples were coimplanted with three different doses, $1 \times 10^{13} / 9 \times 10^{12}$, $1 \times 10^{14} / 9 \times 10^{13}$, $1 \times 10^{15} / 9 \times 10^{14} \text{ cm}^{-2}$ of 200 keV silicon and nitrogen ions, respectively. The samples were annealed at three anneal temperatures, 1250, 1300, and 1350 °C for 29 seconds. These samples were annealed in the Oxy Gon furnace located in the Materials and Manufacturing Directorate of AFRL.

Although extreme precautions were taken to avoid dissociation, the samples from the highest temperature of 1350 °C had complete destruction of the AlN cap layer and also showed liquid gallium on the surface, signifying nitrogen dissociation. Further testing would need to be conducted to determine the cause of the encapsulant failure. The samples from the 1250 and 1300 °C anneals exhibited a small amount of visual damage on the surface. The results of the Hall effect and sheet resistivity measurements made on the GaN samples implanted with various doses at an energy of 200 keV and annealed at 1250 and 1300 °C are shown in Figure 4.1.

The carrier concentration has a dependence upon both the implanted dose and the anneal temperature. The concentration increased as the anneal temperature was increased for all the implanted doses. The highest carrier concentration of $3.54 \times 10^{14} \text{ cm}^{-2}$ was obtained from the sample implanted with $1 \times 10^{15} \text{ Si} / 9 \times 10^{14} \text{ N cm}^{-2}$ and annealed at 1300 °C for 29 seconds.

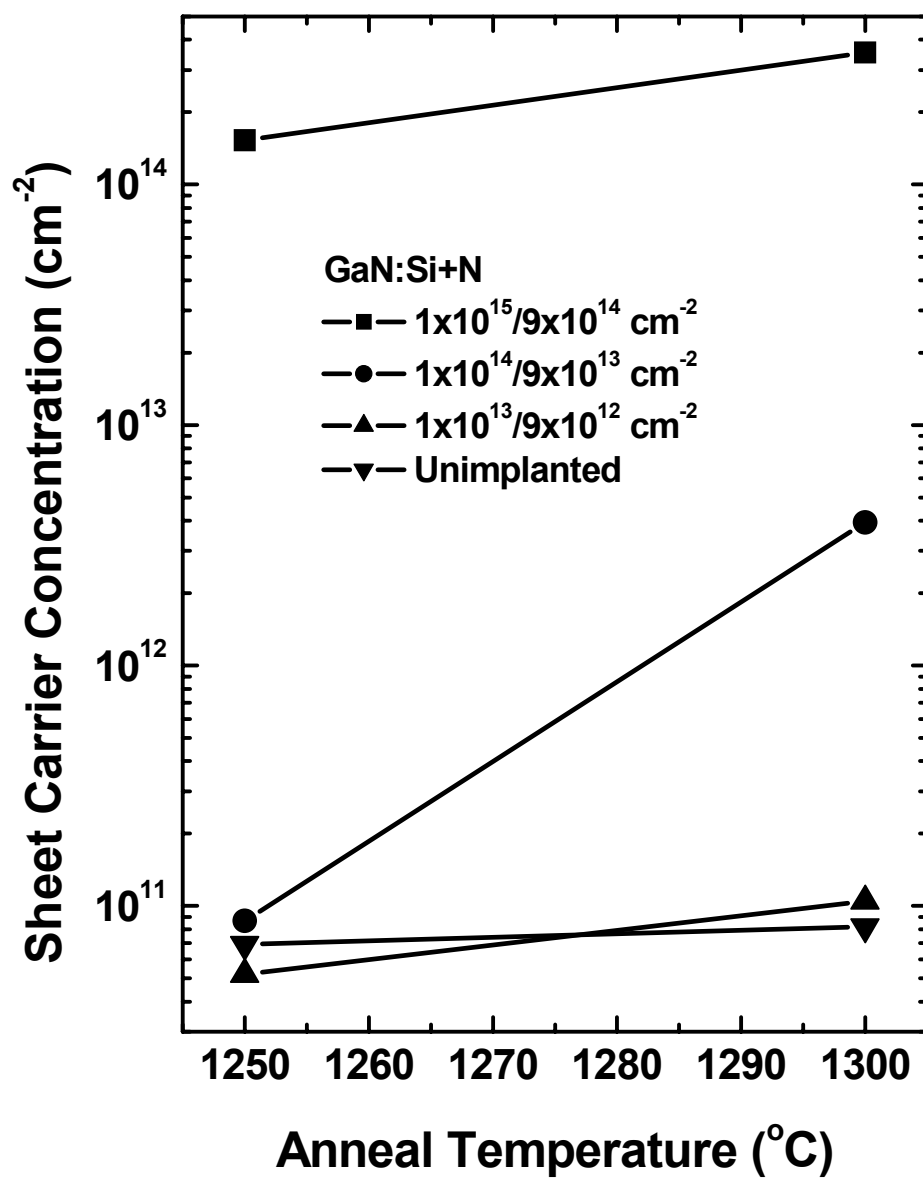


Figure 4.1. Room temperature sheet carrier concentration as a function of anneal temperature for GaN samples coimplanted with various doses and annealed at 1250 and 1300 °C for 29 s.

The sample implanted with the lowest dose of $1 \times 10^{13} / 9 \times 10^{12} \text{ cm}^{-2}$ of silicon and nitrogen respectively, and annealed at 1250°C showed a carrier concentration lower than the unimplanted sample. This is an indication that the crystal damage had not been significantly repaired due to the fact that the anneal temperature may have been too low to electrically activate the implanted ions.

The mobilities for the GaN samples are plotted in Figure 4.2. The lowest implant dose sample displays the highest mobility of $264 \text{ cm}^2/\text{V}\cdot\text{s}$. The mobility increases with the anneal temperature for all implant doses. However, the mobility decreases at higher implant doses. The values of the mobility range from 13.4 to $264 \text{ cm}^2/\text{V}\cdot\text{s}$. This suggests that impurity scattering is significant and also that the higher doses create more crystal damage. The lowest implant dose is the only sample that exhibits a mobility higher than that of the unimplanted sample.

The activations of the coimplanted samples were relatively low as shown in Figure 4.3. The highest activation efficiency obtained was only 37% for the sample annealed at 1300°C for 29 seconds and implanted with a dose of $1 \times 10^{15} \text{ cm}^{-2}$ silicon ions and $9 \times 10^{14} \text{ cm}^{-2}$ nitrogen ions. This is an indication that the radiation damage caused from the implantation was not fully recovered during the annealing process. The anneal temperature might not have been high enough, or the anneal duration might not have been long enough. Since the sample integrity broke down during the 1350°C anneal, it would suggest that the time duration of the anneal might be extended at the lower anneal temperature.

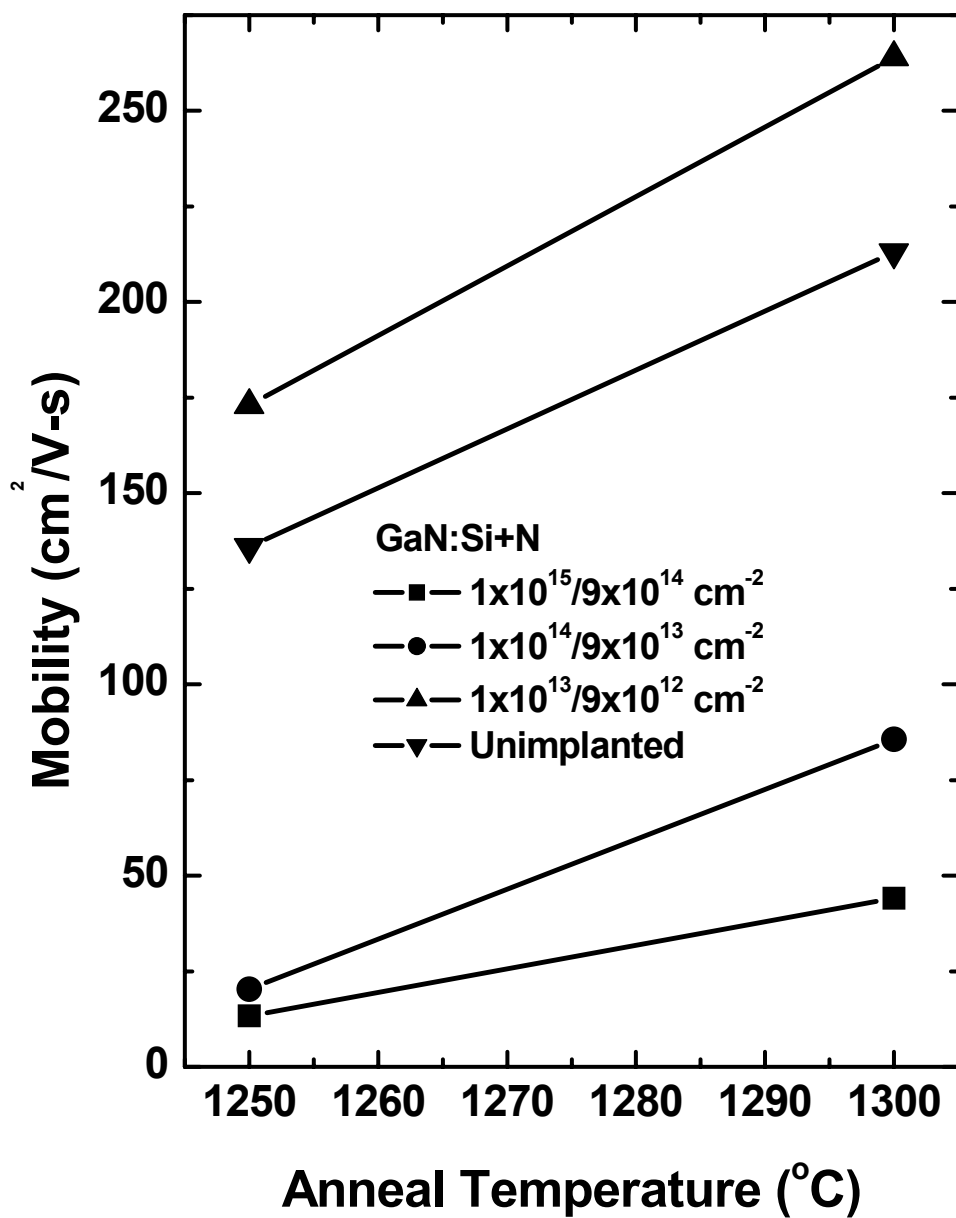


Figure 4.2. Room temperature Hall mobility values for GaN coimplanted with $1 \times 10^{13}/9 \times 10^{12}$, $1 \times 10^{14}/9 \times 10^{13}$, $1 \times 10^{15}/9 \times 10^{14}$ cm⁻² of silicon and nitrogen, respectively and annealed at 1200 and 1300 °C for 29 s.

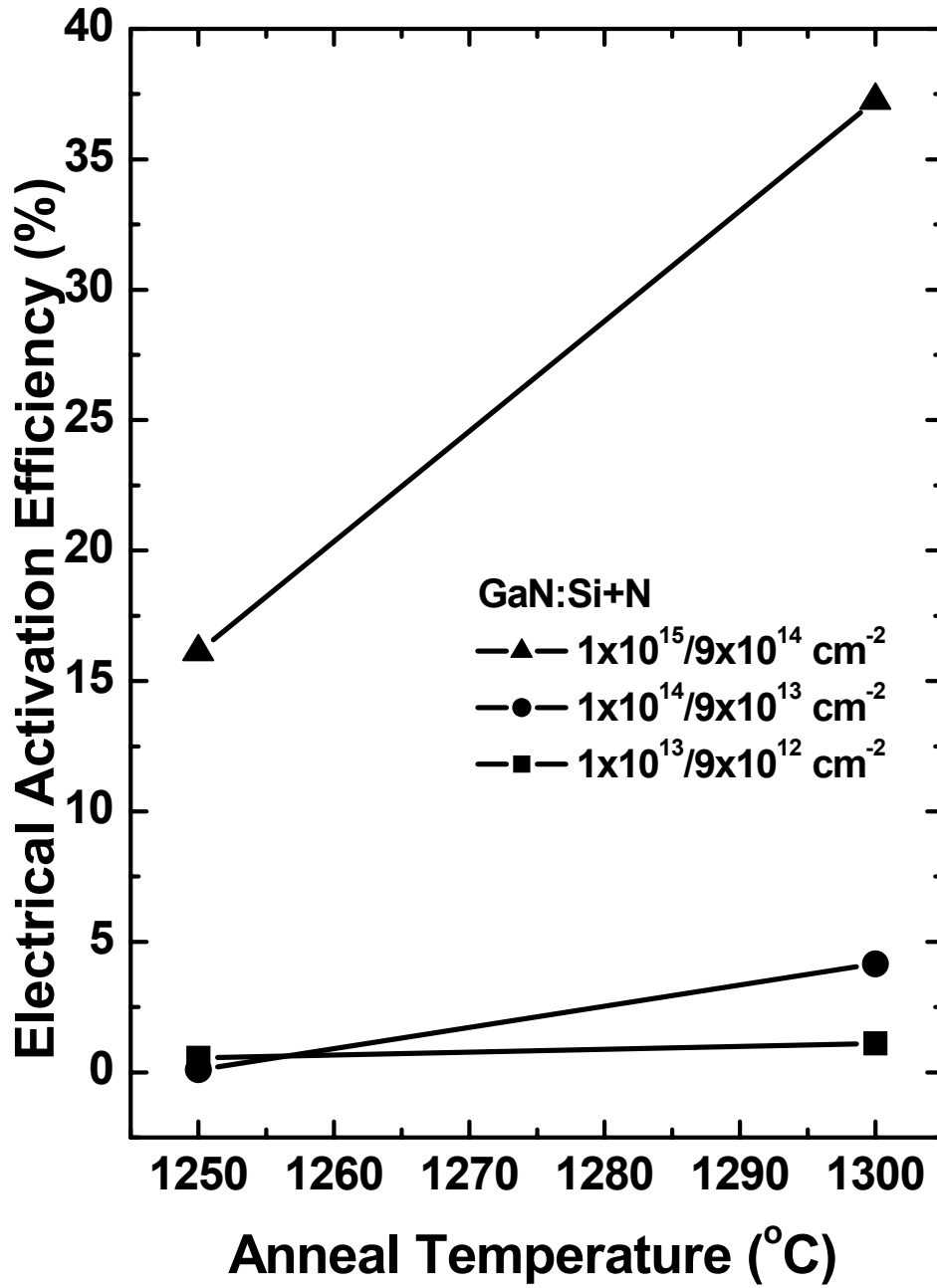


Figure 4.3. The electrical activation efficiency of GaN coimplanted with $1 \times 10^{13} / 9 \times 10^{12}$, $1 \times 10^{14} / 9 \times 10^{13}$, $1 \times 10^{15} / 9 \times 10^{14} \text{ cm}^{-2}$ of silicon and nitrogen, respectively and annealed at 1200 and 1300 °C for 29 s.

Theoretically, it was expected that the Si + N coimplantation could improve the electrical activation of the Si donors. However, the electrical activations for these samples were not as good as were expected. Almost 100% activation has been reported for GaN implanted with $1 \times 10^{15} \text{ cm}^{-2}$ silicon ions at room temperature.¹ The results for all three implanted doses in this study did not turn out as well as those for GaN implanted with silicon alone³. The reasons for this are not clear at present. Somehow, the AlN encapsulant also did not survive as well as expected from previous research.⁵ Further studies are necessary to clarify this problem.

Figure 4.4 is a plot of the carrier concentration as a function of the implanted ion dose. The carrier concentration as well as the activation efficiency increases with the implanted ion dose. The concentration is constant for the two lower-implant dose samples annealed at 1250 °C, and then increases greatly for the highest dose. The constant carrier concentration for these samples might be due to slight damage from the anneal. The samples annealed at 1300 °C show a monotonic increase with the implanted dose.

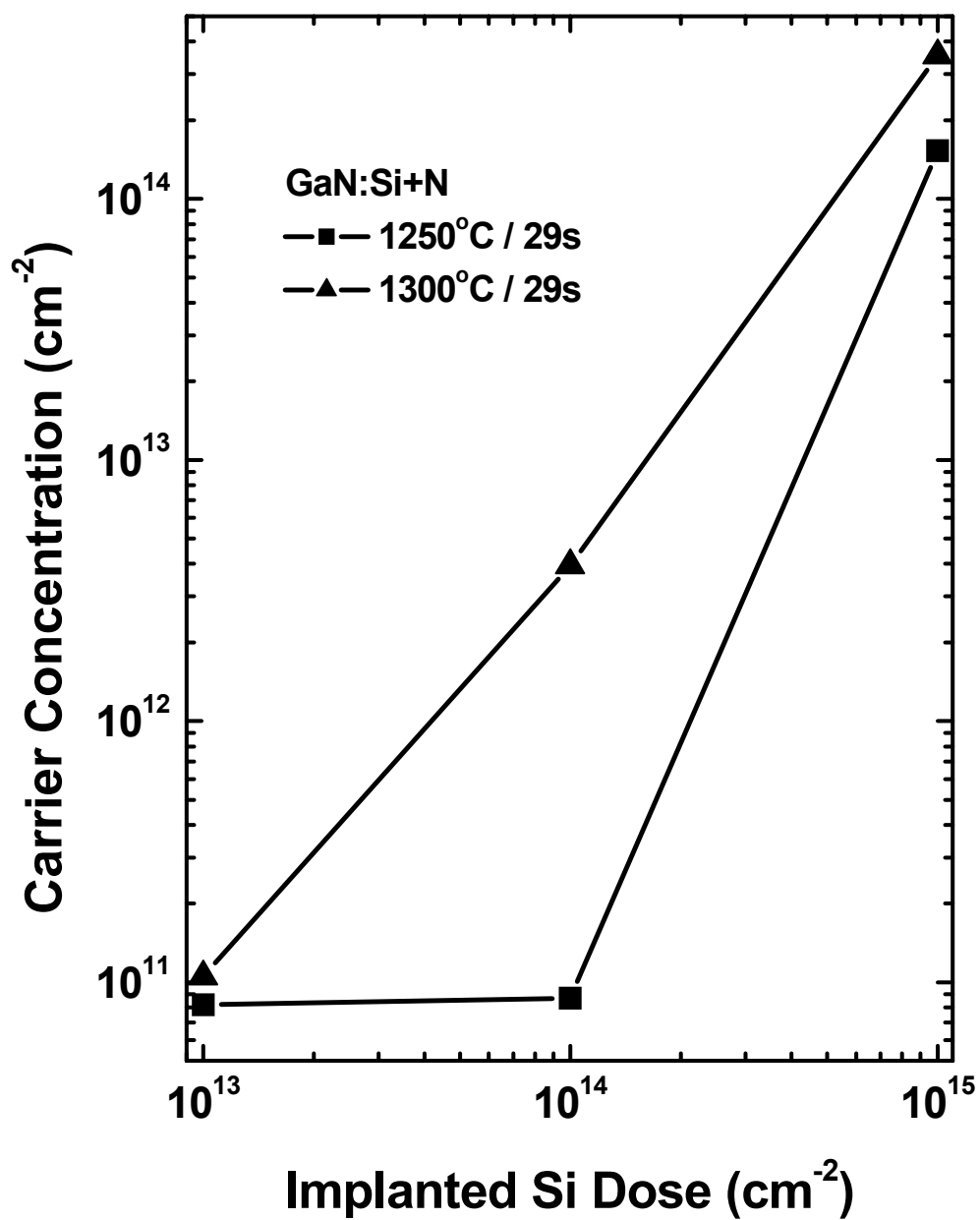


Figure 4.4. Carrier concentration as a function of implanted dose for GaN coimplanted with $1 \times 10^{13} / 9 \times 10^{12}$, $1 \times 10^{14} / 9 \times 10^{13}$, $1 \times 10^{15} / 9 \times 10^{14}$ cm⁻² of silicon and nitrogen, respectively and annealed at 1200 and 1300 °C for 29 s.

4.2 Room Temperature $\text{Al}_x\text{Ga}_{1-x}\text{N}$: Si

The $\text{Al}_{0.2}\text{Ga}_{0.8}\text{N}$ samples were implanted with 200 keV silicon ions at doses of 1×10^{14} and $1 \times 10^{15} \text{ cm}^{-2}$ at room temperature. The $\text{Al}_x\text{Ga}_{1-x}\text{N}$ samples with Al mole fraction of 0.2 were annealed in AFIT's Oxy Gon furnace at four anneal temperatures 1200, 1250, 1300, and 1350 °C for two minutes. The $\text{Al}_{0.2}\text{Ga}_{0.8}\text{N}$ samples implanted with $1 \times 10^{15} \text{ cm}^{-2}$ silicon ions were annealed with AFRL's Oxy Gon furnace at 1300 °C for 29 seconds for comparison. The $\text{Al}_x\text{Ga}_{1-x}\text{N}$ samples with Al mole fraction of 0.3 were implanted with a dose of $1 \times 10^{15} \text{ cm}^{-2}$ and annealed with AFIT's furnace at two anneal temperatures: 1300 and 1350 °C for two minutes.

The carrier concentrations obtained from room temperature Hall effect measurements are shown in Figure 4.5. The carrier concentration has a dependence on the anneal temperature and the implanted dose. As the anneal temperature and implanted dose are increased the carrier concentration increases, similar to the results seen by Fellows.⁵ The carrier concentration declines with increasing aluminum mole fraction. For the sample with Al mole fraction of 0.2, annealed at 1350 °C and implanted with $1 \times 10^{15} \text{ cm}^{-2}$ silicon ions, the sheet carrier concentration obtained was $8.2 \times 10^{14} \text{ cm}^{-2}$. The highest carrier concentration exhibited for the samples with 0.3 aluminum mole fraction was $4.04 \times 10^{14} \text{ cm}^{-2}$ on the sample annealed at 1300 °C and implanted with $1 \times 10^{15} \text{ cm}^{-2}$. The carrier concentration for the aluminum mole fraction of 0.3 is relatively constant for both anneal temperatures of 1250 and 1300 °C, suggesting that the higher temperature anneal may not have been necessary with regard to carrier concentration.

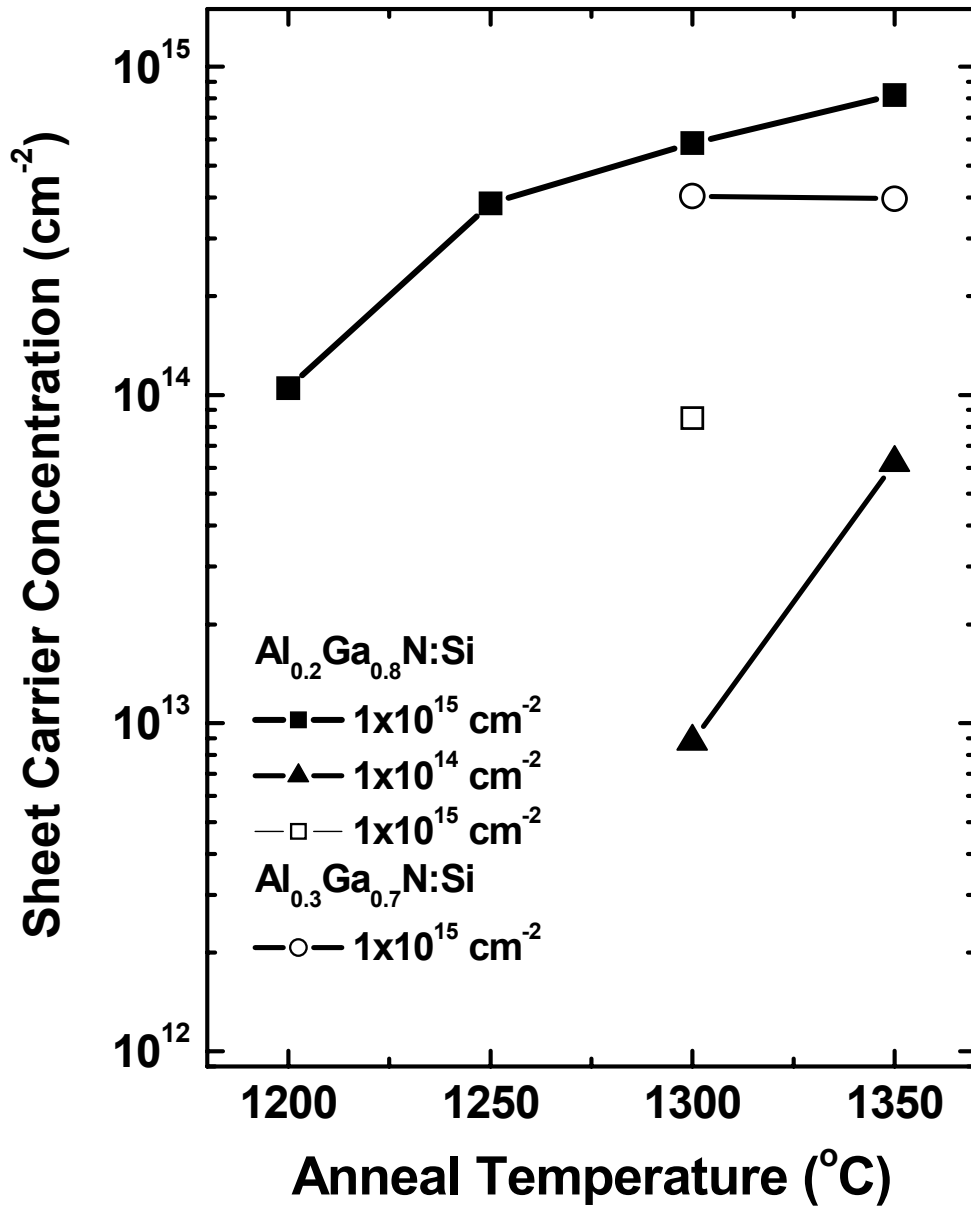


Figure 4.5. Carrier concentrations from room temperature Hall data as a function of anneal temperature for $\text{Al}_x\text{Ga}_{1-x}\text{N}$ implanted with silicon at various doses and annealed from 1200 to 1350 °C. All the samples were annealed for 120 s in AFIT's Oxy-Gon furnace, except for the sample indicated by \square , which was annealed at AFRL for 29 s.

The carrier concentrations increased with anneal temperature. The two samples with aluminum mole fraction of 0.2, implanted with $1 \times 10^{15} \text{ cm}^{-2}$ silicon ions and annealed at 1300°C for 120 seconds and 29 seconds respectively, show a dramatic difference in carrier concentration. The sample annealed for 120 s has a carrier concentration of $5.85 \times 10^{14} \text{ cm}^{-2}$. This is much higher value than that recorded for the 29 s anneal, which has a carrier concentration of $8.3 \times 10^{13} \text{ cm}^{-2}$. The sample annealed for longer time duration exhibits improvement in carrier concentration.

The increase in mobilities with anneal temperature and implanted ion dose can be seen in Figure 4.6. There is an only slight increase in mobility for the samples with aluminum mole fraction of 0.3 as the anneal temperature increases. The two samples annealed at 1300°C with aluminum mole fraction of 0.2 have different results. The longer anneal time for the sample implanted with $1 \times 10^{15} \text{ cm}^{-2}$ silicon ions produced a mobility of $33.2 \text{ cm}^2/\text{V}\cdot\text{s}$ while 29 s anneal utilizing the AFRL furnace and same sample conditions has a mobility of $5.7 \text{ cm}^2/\text{V}\cdot\text{s}$. The longer time duration may have allowed for more of the crystal damage to be repaired and thus decrease lattice scattering. The mobilities for these samples are generally low. There is not a clear relationship between the mobility and aluminum mole fraction. At 1300°C , the samples with a higher mole fraction exhibit a higher mobility. While the reverse is true for the 1350°C anneal. This is because the mobility depends on both impurity and lattice scattering. This signifies that there is still crystal damage that is impeding the movement of the electrons for the samples annealed below 1350°C .

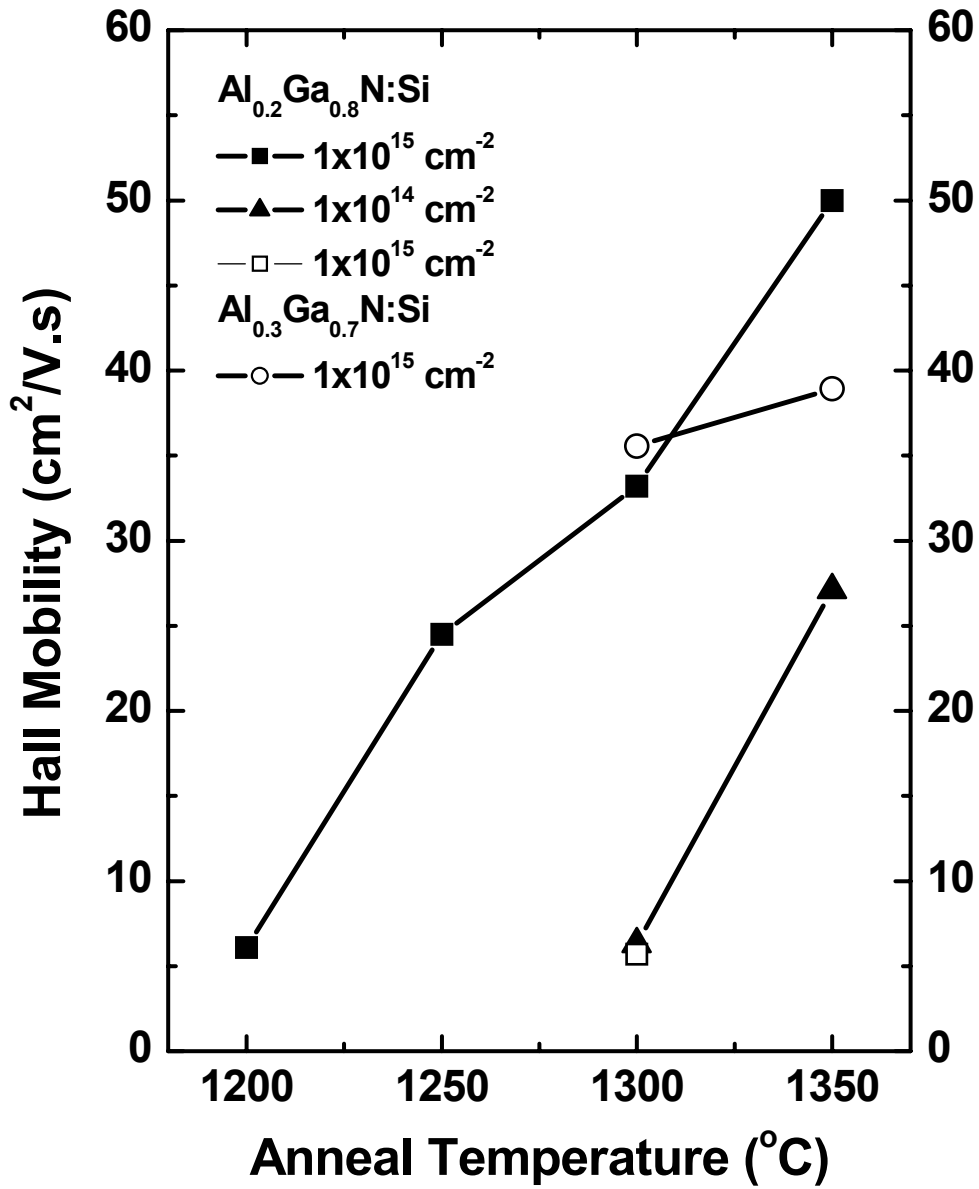


Figure 4.6. The mobility values from room temperature Hall data for $\text{Al}_x\text{Ga}_{1-x}\text{N}$ implanted with silicon at various doses and annealed from 1200 to 1350 °C. All the samples were annealed for 120 s in AFITs Oxy-Gon furnace, except for the sample indicated by \square , which was annealed at AFRL for 29 s.

The mobility improves with the anneal temperature and exhibits a maximum of 50 $\text{cm}^2/\text{V}\cdot\text{s}$ for the sample implanted with $1 \times 10^{15} \text{ cm}^{-2}$ and annealed at 1350 °C for 120 s. The observed low mobility for the sample annealed at 1350 °C may be primarily due to impurity scattering by higher carrier concentrations. Also, the crystal damage increases the concentration of scattering centers that act to greatly decrease the mobility of the electrons. The type of defects in the crystal may be determined through photoluminescence, cathodoluminescence, or other methods.

The electrical activation efficiencies of the $\text{Al}_x\text{Ga}_{1-x}\text{N}$ samples are plotted as a function of anneal temperature in Figure 4.7. The activation increases with the anneal temperature for all the implanted doses with 0.2 Al mole fraction. The samples with 0.3 Al mole fraction have relatively constant activation efficiencies for both anneal temperatures. The sample with 0.2 Al mole fraction and annealed for 29 seconds at 1300 °C had only 10% activation, while the sample with the same conditions annealed for 120 s exhibited about 62% activation. The highest activation efficiency obtained was almost 90% for the sample annealed at 1350 °C and implanted with $1 \times 10^{15} \text{ cm}^{-2}$ silicon ions. The samples with 0.2 aluminum mole fraction annealed for two minutes exhibit a monotonic increase in activation efficiency with anneal temperature.

The electrical activation efficiency is calculated using the effective ion dose. The removal of the 500 Å AlN encapsulant also removes about five percent of the implanted ions. The efficiency increases almost linearly with the anneal temperature. For the lowest temperature anneal at 1200 °C, the activation is only about 10% and then the

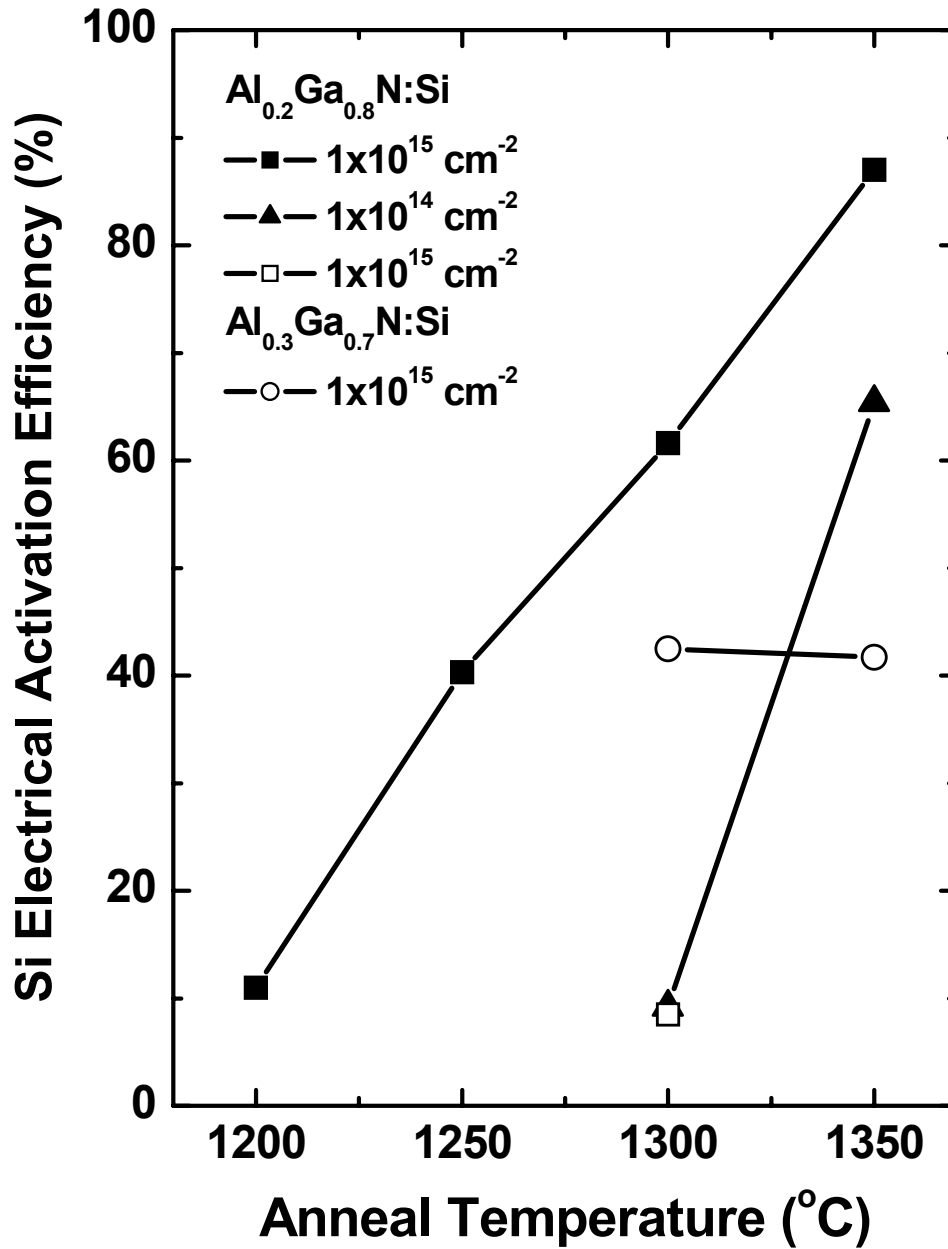


Figure 4.7. The electrical activation efficiencies for Al_xGa_{1-x}N implanted with doses of 1x10¹⁴ and 1x10¹⁵ cm⁻² silicon ions and annealed from 1200 to 1350 °C. All the samples were annealed for 120 s in AFITs Oxy-Gon furnace, except for the sample indicated by □, which was annealed at AFRL for 29 s.

activation increases to almost 90% for the 1350 °C anneal, which is the highest reported activation in $\text{Al}_{0.2}\text{Ga}_{0.8}\text{N}$, to the best of our knowledge.

4.3 Temperature Dependent $\text{Al}_{0.2}\text{Ga}_{0.8}\text{N}$: Si

Temperature dependent Hall measurements were also carried out for the $\text{Al}_{0.2}\text{Ga}_{0.8}\text{N}$ sample implanted with Si at 200 keV with a dose of $1 \times 10^{15} \text{ cm}^{-2}$ and annealed at temperatures of 1250, 1300 and 1350 °C. The Hall measurements were taken over the temperature range of 10 to 320 K.

The results for the carrier concentration as a function of temperature can be viewed in Figure 4.8. The sheet carrier concentrations for all three anneal temperatures remain relatively constant up to about 70 K and then increase slightly with the sample temperature. The constant nature of the carrier concentration at low temperature suggests that the sample is highly degenerate. As the temperature is increased, the electrons gain the thermal energy required to jump the energy gap into the conduction band, thus increasing the carrier concentration of the sample.

The mobilities for all three anneal temperatures exhibited the same dependence on the temperature shown in Figure 4.9. The mobilities remain relatively constant over much of the temperature range and increase monotonically up to the highest temperature investigated, 320 K.

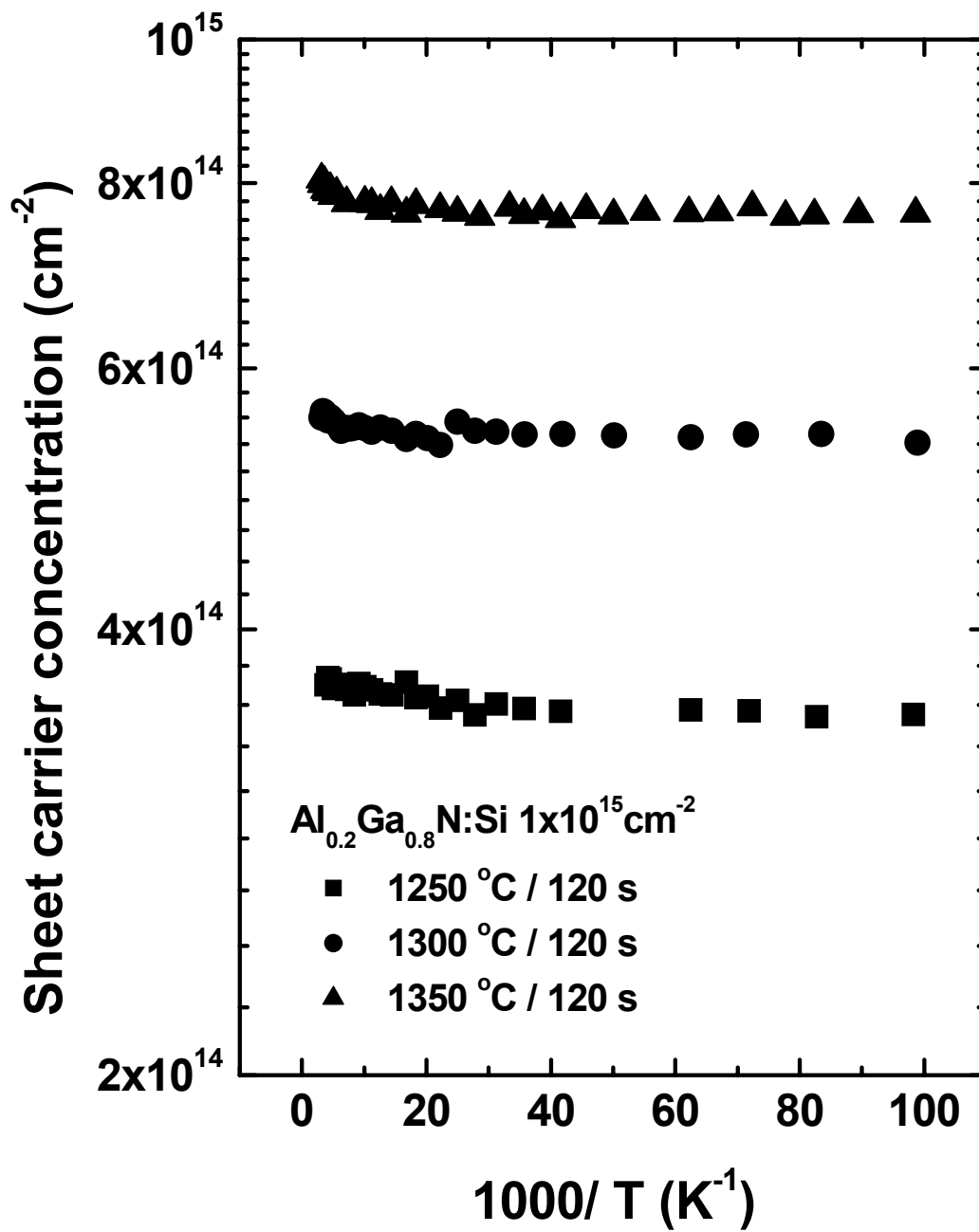


Figure 4.8 The temperature-dependent sheet carrier concentrations taken from 10 – 320 K for $\text{Al}_{0.2}\text{Ga}_{0.8}\text{N}$ implanted with 1×10^{15} silicon ions/ cm^2 and annealed at 1250, 1300 and 1350 °C for 120 s.

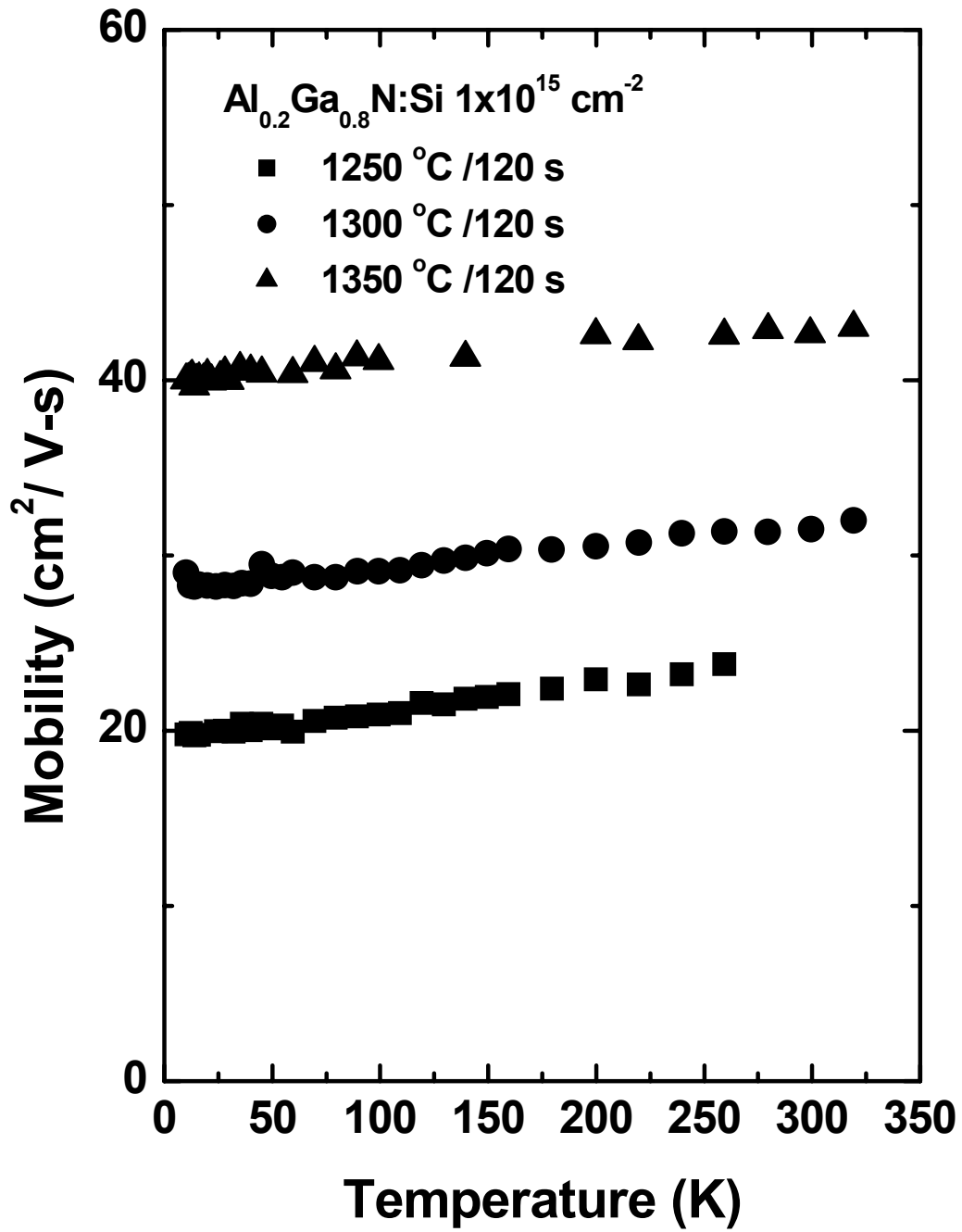


Figure 4.9 The temperature-dependent Hall mobility values taken from 10 – 320 K for $\text{Al}_{0.2}\text{Ga}_{0.8}\text{N}$ implanted with 1×10^{15} silicon ions/cm² and annealed at 1250, 1300 and 1350 °C for 120 s.

The constant behavior of the mobility implies that a degenerate impurity band has been formed. The degenerate impurity band affects all samples. The mobilities show no considerable decrease at increased temperatures.

Figure 4.10 shows that the resistivity is constant over much of the temperature range. At higher temperatures the resistivity begins to decrease dramatically in particular for the sample annealed at 1250 °C. The degenerate impurity band affects the resistivity as well. Not until the temperature reaches around 100 K does the resistivity begin to show any dependence on the temperature for the high temperature annealed samples. At this point, the resistivity begins to decrease quickly, reaching its lowest point at the highest temperature evaluated, 320K.

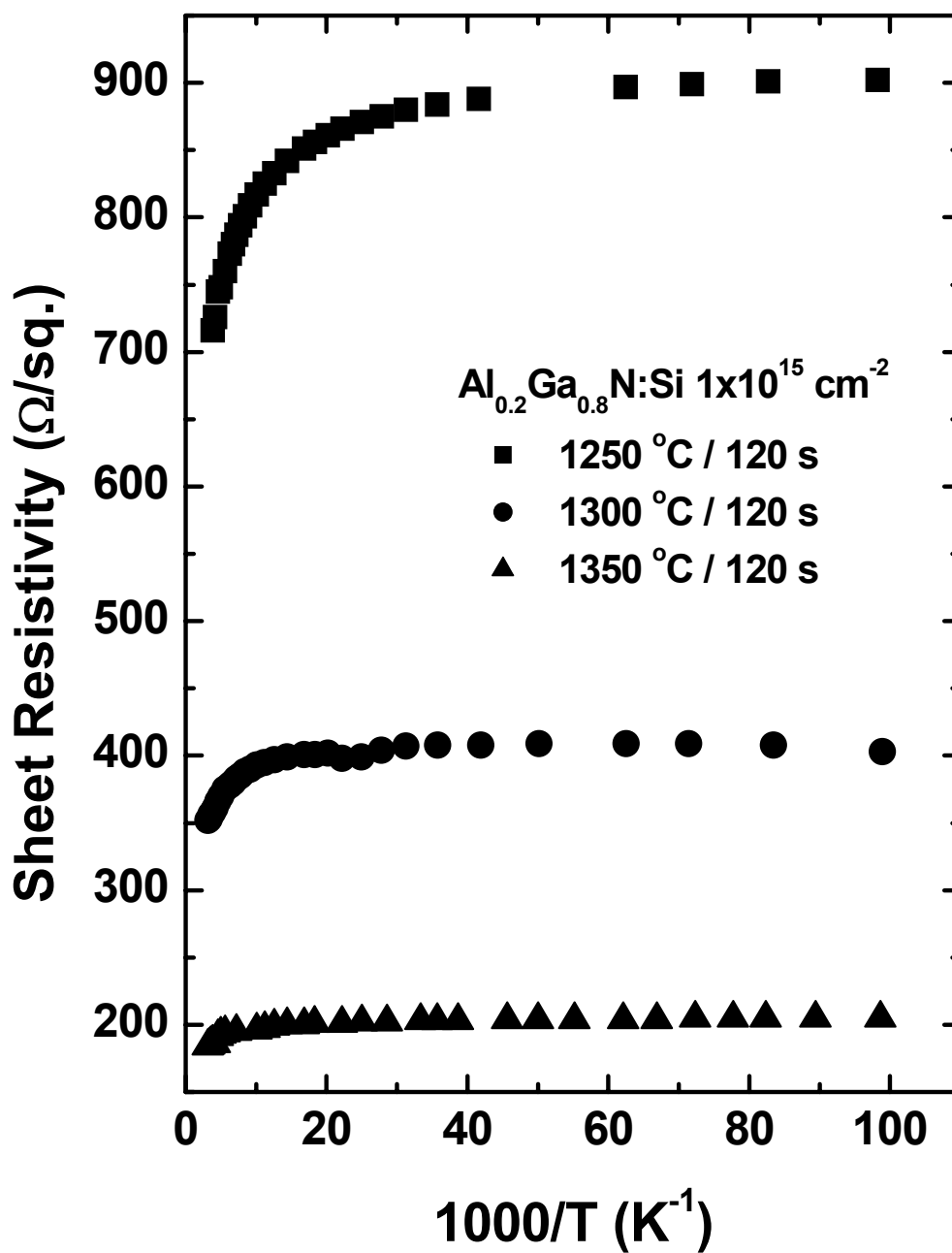


Figure 4.10 The temperature-dependent sheet resistivity data taken from 10 – 320 K for Al_{0.2}Ga_{0.8}N implanted with 1x10¹⁵ silicon ions/cm² and annealed at 1250, 1300 and 1350 °C for 120 s.

5. Conclusions

The objective of this research was to perform a systematic study of the electrical properties of silicon implanted $\text{Al}_x\text{Ga}_{1-x}\text{N}$ and coimplanted GaN as a function of anneal temperature and implanted ion dose. The secondary motivation was to investigate the electrical properties of silicon implanted $\text{Al}_x\text{Ga}_{1-x}\text{N}$ as a function of aluminum mole fraction. For both studies, the optimum anneal temperature was sought.

The GaN substrates were encapsulated with 500 Å of AlN and implanted at room temperature with doses ranging from 1×10^{13} / 9×10^{12} to 1×10^{15} / 9×10^{14} cm^{-2} of silicon ions and nitrogen ions, respectively. They were annealed at temperatures from 1250 to 1350 °C for 29 seconds in a flowing nitrogen environment. Room temperature Hall effect measurements were conducted to measure the Hall coefficient and resistivity. The Hall mobility, sheet carrier concentration, and electrical activation efficiency were determined.

The coimplantation of the GaN did not produce the expected results and the electrical properties were in fact hindered by the coimplantation. It was hoped that the second implant species would help the electrical activation of the semiconductor material. The mobilities of these samples did not appear to be affected by the coimplantation. The optimum anneal temperature cannot be determined from the given data. It would appear that this temperature is around 1300 °C, but the anneal time should be extended. The best

results came from the sample annealed at 1300 °C and implanted with a dose of 1×10^{15} cm⁻² of silicon ions and 9×10^{14} cm⁻² of nitrogen ions with an activation efficiency of 42%.

The AlGa_N substrates were encapsulated with 500 Å of AlN and implanted at room temperature with doses ranging from 1×10^{13} to 1×10^{15} cm⁻² of silicon ions. These samples were annealed at four temperatures (1200, 1250, 1300 and 1350 °C) for two minutes using AFIT's Oxy Gon furnace and at one temperature (1300 °C) for 29 seconds with AFRL's Oxy Gon furnace. Room temperature Hall effect measurements determined the carrier concentration, mobility and resistivity of the samples. The highest activation efficiency was found to be 90% on the sample with 0.2 Al mole fraction implanted with 1×10^{15} cm⁻² silicon ions. TDH measurements were also conducted on the Al_{0.2}Ga_{0.8}N to further investigate its characteristics as a function of temperature.

The Al_xGa_{1-x}N samples with Al mole fraction of 0.3 show about 42% activation for both anneal temperatures of 1300 and 1350 °C. The results did not improve with increased anneal temperatures, so extending the duration of the anneal might repair more of the radiation damage.

The Al_xGa_{1-x}N samples with Al mole fraction of 0.2 exhibited the best results. An activation efficiency of almost 90% was achieved with the sample implanted with 1×10^{15} cm⁻² of silicon ions and annealed for 120 s at 1350 °C. The 90% activation suggests that 1350 °C is nearly the optimum anneal temperature for this implanted ion dose. The

$\text{Al}_{0.2}\text{Ga}_{0.8}\text{N}$ samples are highly degenerate samples. The activation efficiency increases with anneal temperature up through 1350°C .

Appendix A

The procedures for sample preparation were taken from Major Jim Fellows' Dissertation.⁵

Sample Cutting and Cleaning Procedures

Cleanroom:

1. Turn solvent hood hotplate ON and set to 100 °C.
2. Place clean 3" Si wafer face-up on hotplate.
3. Place as many 1¼" ceramic cutting disks face-down on hotplate as you have source wafers to cut.
4. Label a glassine envelope for each 5 mm x 5mm sample you expect to cut.
5. Place source wafer on appropriate-sized spinner vacuum chuck, spin wafer and clean with acetone, methanol, blow dry w/N₂.
6. Cover entire surface of source wafer with 1813 photoresist using dropper and spin on at 4000 rpm for 30 sec.
7. Place PR covered wafer face up on Si wafer for 4 min.
8. At 4 min mark, flip source wafer over and melt crystal bond onto backside ensuring edge from which samples will be cut has full coverage. Note: avoid getting crystal bond on Si wafer—this will make the mounting process go much smoother.
9. Immediately touch the face of a 1¼" ceramic cutting disk to the crystal bond coated wafer surface and lift. If wafer is stuck to Si wafer, carefully loosen with tweezers and reattempt bonding. If wafer bonds to disk, set aside to cool. Uniquely identify each ceramic disk. *** **Write down which disk has which source wafer!!!** ***
10. Repeat steps 5-9 for each source wafer to be cut.
11. Place all mounted wafers in transport box along with tweezers, crystal bond, and the brass mounting ring.
12. Turn OFF hotplate and remove Si wafer.
13. Place Si wafer on appropriate-sized spinner vacuum chuck, spin wafer and clean with acetone, methanol, blow dry w/N₂.

Wiresaw:

14. Carry box to wire saw room and turn on hotplate in fume hood on very lowest temperature.
15. Ensure there is adequate distilled drip water for wire saw.
16. Securely mount a disk on the wire saw pedestal.
17. Align wire parallel to sample edge to be cut so that wire is just barely not touching sample.
18. Once wire and sample are properly aligned, activate and zero the sliding micrometer.
19. Lower saw swing arm and slide sample tray until micrometer reads ± 5.18 mm.
20. Set appropriate drip rate; position drip spot over sample and wire.
21. Turn ON saw motor, and set to 50%.
22. Cut sample slice. When wire is almost through sample minimize pressure between sample and wire to prevent uneven cutting or chipping of sapphire substrate.
23. Lower swing arm, turn saw to 0%.
24. Secure swing arm, remove ceramic disk and place face-up on hotplate until the next wafer has been cut.
25. Repeat steps 16-24 for next source wafer to be cut.

26. Once crystal bond has been sufficiently softened on previously cut wafer, carefully remove the portion of source wafer that will not be cut into samples, remembering its ID.
27. Repeat steps 16-23 for each strip that will be cut into square samples; make initial wire alignment with the end of the strip that is closest to the center of the grown wafer—in some cases this requires remembering the location of the wafer flat.
28. After each square sample is cut, zero the micrometer and slide the sample tray ± 5.18 mm until end of strip is reached; continue until all samples are cut, keeping careful track of which pieces belong to which wafer.
29. Lower and secure saw swing arm, turn OFF saw; turn OFF hotplate.

Cleanroom:

30. Return to cleanroom and turn solvent hood hotplate ON and set to 100 °C; Place all cutting disks face-up on hotplate
31. Set out as many 2” diameter pitri dishes with covers as you have source wafers and fill each $\sim\frac{1}{3}$ full w/ acetone.
32. Once crystal bond has been sufficiently softened, carefully remove each sample and place all pieces from each source wafer in their own pitri dish *** **Organization is crucial to keeping track of which samples are which!** ***
33. Once all the pieces are soaking in covered dishes of acetone, turn OFF the hotplate.
34. Add DI water to each dish with a ratio of acetone:DI of about 3:1 to aid in removing the ceramic disk residue.
35. Fill the ultrasonic cleaner with DI water to the level of fluid in each pitri dish.
36. Place each dish in the ultrasonic cleaner simultaneously ONLY if you can tell them apart, and ultra for 20 seconds.
37. Remove dishes from the cleaner; carefully flush each dish with clean acetone and cover.
38. Clean each piece one at a time—holding with tweezers, rinse with acetone, methanol, and DI water, blowing dry w/N₂ and immediately placing in the appropriate glassine envelop prepared beforehand.
39. Once all the samples and remaining source wafers (and remnants) have been cleaned and packaged, clean all quartzware with acetone and methanol--wiping will likely be necessary due to the PR, crystal bond and ceramic residue.

Oxy-Gon Sample Preparation Procedures

1. Select all the 5 mm x 5mm samples (which were previously cut & cleaned) you'll anneal.
2. On the cleanroom table, place a clean 3” Si wafer on a cloth wipe.
3. While holding them face down on the Si wafer, uniquely scribe the Al₂O₃ backside of each sample type (e.g., “ / “, “ < ”, “ | “, “O”, “L”, etc.)
4. Logically (e.g. hot and cold of same dose) and physically (e.g., best size match) pair up the samples.
5. After scribing, place all samples to be annealed in a 2” pitri dish for temporary storage and transport.
6. Measure out $\sim 1\frac{3}{4}$ ” of Ta-wire for each sample pair to be annealed, cutting one long piece.
7. Place this single piece of Ta-wire in a 2” pitri dish, submerge the wire in TCE, and cover the dish.
8. Clean all samples again (front and back) with acetone and methanol rinses (and, as necessary to fully remove ceramic disk residue and make each surface mirror-like, DI H₂O), blow dry with N₂.

9. Rinse and flush the Ta-wire in the dish with acetone, then methanol. While still wet, pull the wire between a clean cloth wipe to dry.
10. Cut the wire into 1 $\frac{3}{4}$ " sections.
11. Identify which samples will be wrapped face-to-face noting which sample will be on top.
12. Note: Practicing this process several times on a pair of junk samples is recommended.
13. Place a piece of Ta-wire on a cloth wipe and center the face-to-face samples in the middle of the wire.
14. Using two sets of tweezers, press the center of the samples together while wrapping the ends of the wire up and back across the top of the samples.
15. Bend first one end of the wire 90° at the center of the samples across the other wire, then bend the other end 90° so they interlock (like string on a Christmas package, or twine on a bail of hay).
16. Flip the sample pair over and repeat steps 14-15.
17. Flip the sample pair over and repeat steps 14-15 again, at which point you should have just enough wire to complete the final bends (step 15), only here interlock the ends and bend 180° vice 90°.
18. Keep the samples fully face-to-face throughout the process and wrap them securely. Any uncovered regions along the edge will be destroyed by the anneal—the samples must overlap perfectly!
19. Place the sample pair in the glassine envelope of the sample that started (and finished) on top.
20. Repeat steps 13-19 for each sample pair.
21. Place all the glassine envelopes in a plastic box and double bag for transport to anneal furnace.
22. Be sure to bring tweezers, gloves, wipes, and a metal dish for transport to/from the furnace.

Oxy-Gon AlN/GaN Anneal Procedures

System Start-Up (process selection switch should be in **STANDBY**):

1. Turn **ON** 80 psig house air (vent and vacuum valves are air pressure activated)
2. Turn **ON** Main Power switch (handle on lower front panel)
3. Turn Roughing pump **ON** (green button); Roughing pulls on Turbo to 10⁻³ Torr
4. Turn Turbomolecular pump **ON** (green button); Turbo pulls on itself
5. If chamber is still under a vacuum, turn process selection switch to **VENT GAS**, else GOTO 8
6. Turn **ON** low-O₂ N₂ at tank and regulator; ensure ball valve on furnace works
7. When chamber reaches atmospheric pressure, Turn **OFF** low-O₂ N₂ or Ar at tank and regulator
8. **Open** chamber, propping door open with ruler as necessary
9. **Inspect** graphite elements and electrodes for discoloration/wear; carefully **wipe** off any condensation or residue from walls
10. **Remove** previous samples as necessary and **insert** new samples evenly spaced in center of puck, then **secure** chamber door

Soft Bake (to remove impurities from hot zone):

11. Turn process selection switch to **STANDBY**, then **ROUGH**
12. Turn **ON** Ion Gauge Controller to read TCs
13. Rough pump until chamber is mid 10⁻² Torr (read TC2); this will take a few minutes; Turbo still pulls on itself, and pressure increases slightly at TC1

14. Turn process selection switch to **HI VACUUM** (Turbo pulls on chamber, Rough pulls on Turbo—TC2 drops quickly; TC1 increases then drops more slowly)
15. To remove trapped O₂ between GaN samples, **Repeat** steps 5 through 7 only, and begin again at step 11
16. Turn **ON** Ion Gauge Filament when TC2 is in the 10⁻³ Torr range, & pump until mid-high 10⁻⁵ Torr
17. After ~10 min into 2nd Hi-vac pull, **Open** H₂O inlet and outlet hand valves (only when chamber under vac. or filled with N₂)
18. Ensure yellow H₂O handles are open: 2, 4 & Chamber Main at 45°, 1 & 3 at full open, and H₂O safety light is ON.
19. **RESET** Over Temperature Controller to start pre-anneal soft bake of elements and chamber
20. Ensure Vacuum Interlock Bypass is OFF, Turn Heat Zone **ON**
21. Approx. 5 min after H₂O on, ion gauge should be mid-hi 10⁻⁵ Torr; **Ramp Up** AUTO/MAN power controls to 20%
22. Soft Bake chamber at 20% for 12 min (expect T to be approx. 230 °C; if significantly less, TC may be bad—abort run ***)
23. **Ramp Down** AUTO/MAN power controls to 8% and continue softbake for another 5 min
24. **Ramp Down** AUTO/MAN power controls to 0%
25. Turn **OFF** Ion Gauge Filament (Heat Zone may go off simultaneously) ensuring P ~mid-hi 10⁻⁵ Torr

Set-Up Anneal Environment:

26. Turn **ON** low-O₂ N₂ or Ar at tank and regulator
27. Turn process selection switch to **VENT GAS** to backfill chamber to ~1 PSIG
28. Adjust vent floating ball valve so that chamber gas is just barely flowing

Anneal Process:

29. Turn **ON** Vacuum Interlock Bypass (and turn **ON** Heat Zone as necessary)
30. **Ramp Up** AUTO/MAN power controls for desired temperature profile (55% initially for graphite to minimize excessive current, then gradually up to 69% max at T ≥ 1150 °C to maximize ramp rate). *Carefully* control power to not overshoot.
31. ANNEAL GaN samples
32. At appropriate time, **Ramp Down** AUTO/MAN power controls to 0%
33. Using floating ball valve, gently increase vent gas flow rate to the 10-15 lpm range
34. Turn **OFF** Heat Zone 10 min into cool-down (after power supply has cooled) on last run
35. Turn **OFF** Turbo during last run of the day
36. **Close** H₂O inlet and outlet hand valves, respectively, when T < 100 °C
37. When chamber reads T < 30 °C (for AlN/GaN), **Close** floating ball valve, Turn **OFF** low-O₂ N₂ at tank and regulator
38. If annealing more samples, GOTO 8
39. **Open** chamber, propping door open with ruler as necessary, carefully **remove** samples, then **secure** chamber door

System Shut Down:

40. Turn process selection switch to **STANDBY**, then **ROUGH**
41. Rough pump until TC2 ~ mid 10⁻² Torr, if Turbo is still on, Turn process selection switch to **HI VACUUM** until TC2 ~ 10⁻³
42. If short term shut down (< 1 day), Turn process selection switch to **STANDBY**, Turn **OFF** Turbo, GOTO 45

43. Turn process selection switch to **VENT GAS**, and **Open** floating ball valve to backfill chamber to ~1 PSIG
44. **Close** floating ball valve; Turn process selection switch to **STANDBY**
45. Turn **OFF** vent gas at tank and regulator
46. Turn **OFF** Vacuum Interlock Bypass
47. Turn **OFF** Roughing pump
48. Turn **OFF** Ion Gauge Controller
49. Turn **OFF** Main Power switch
50. Turn **OFF** 80 psi house air

Post-Anneal Contact Preparation Procedures

1. Obtain HCl and HNO₃ acids and place within the acid fume hood.
2. Turn ON one solvent fume hood hotplate and set to 140 °C.
3. Turn ON the second solvent fume hood hotplate and set to 90 °C.
4. On the cleanroom table, place an annealed Ta-wire-wrapped sample pair on a clean cloth wipe.
5. Using two sets of tweezers, carefully break off the brittle Ta wire-wrap, keeping track of which sample is which throughout the process.
6. Visually examine the AlN surface for signs of Ga droplets, cracking/peeling etc. (A good AlN surface post anneal will be as mirror-like as when it was wrapped.)
7. If the identifying scribe markings on the backside are no longer clearly distinguishable (at any angle or over a reflective Si wafer) place the sample on a clean 3" Si wafer and re-scribe.
8. Place the samples in a 2" pitri dish for temporary storage and transport.
9. Fill a clean 250 ml quartz beaker with 50 ml of DI H₂O; cover and place on the 140 °C hotplate.
10. Repeat steps 4-8 for each sample pair you have annealed.
11. Weigh out 1.63 g of KOH pellets (86% KOH) and tightly close the double bag.
12. Quickly place all pellets into the beaker of hot DI H₂O as the pellets will begin to melt in air.
13. Stir with tweezers until all pellets are fully dissolved and cover the beaker. (Although the hotplate is set at 140 °C, the DI H₂O will not boil, typically reaching at most 95 °C.)
14. *** Note: ensure the evaporator is not in use before proceeding with any acid processing.
15. Measure out 30 ml of HCl and place in a clean 250 ml quartz beaker.
16. Measure out 10 ml of HNO₃ and add to the HCl; gently circulate and cover the aqua regia.
17. Process ONLY the good morphology samples as the first batch (< 5-10% total metallic Ga surface area is good). Process all other samples in the second batch.
18. Place each sample in the 0.5M hot KOH solution; starting a 5 min timer on the first sample.
19. Continue placing samples one at a time at the same rate in the KOH sequentially along the circumference of the beaker and cover when finished.
20. When the samples have only 1 min left in the KOH, bring the covered beaker of aqua regia to the solvent fume hood and place on the 90 °C hotplate.
21. At 5 min, remove the samples at the same rate and in the same order in which you inserted them.
22. As each sample is removed, place it into a large (600 ml) beaker of clean DI H₂O.

23. Carefully rinse the samples in the beaker by dumping most of the DI/adding clean DI, dumping/adding—taking care to not even come close to loosing any samples. Leave at most 1" of DI in beaker.
24. When the aqua regia just begins to boil, place the samples into the acid solution directly from the DI beaker; starting a 2 min timer on the first sample.
25. Continue placing samples one at a time at the same rate in the aqua regia sequentially along the circumference of the beaker and cover when finished.
26. At 2 min, remove the samples at the same rate and in the same order in which you inserted them.
27. As each sample is removed, place it into a large beaker of clean DI H₂O.
28. When all the samples are in the DI, cover the aqua regia and turn off the 90 °C hotplate.
29. At this point, you may need to rinse a green residue off the metal tweezers, wipe, rinse and blow dry with N₂
30. Carefully rinse the samples in the beaker by dumping most of the DI/adding clean DI, dumping/adding—taking care to not even come close to loosing any samples. Leave at most 1" of DI in beaker.
31. Holding with tweezers, agitate each sample in the DI, remove, blow dry with N₂ and place in a clean 2" pitri dish.
32. Repeat steps 18-31 for the second batch as necessary using the same acid and base solutions.
33. On the cleanroom table, carefully mount all samples face down on the van der Pauw shadow mask on a clean cloth wipe.
34. Adjust and secure each sample by gently tightening mounting screws until all samples are positioned for contacts as much in the corners as possible.
35. Note: Each row on the mask is a different sized square; generally the largest two square rows are best.
36. *** Note: This is an iterative and tedious process as tightening one sample may loosen another. ***
37. When all samples are securely squared, vent the evaporator and carefully insert the mask.
38. Remember to change the microscope window slides, check metal levels, secure door and "process".
39. Turn off both hotplates, clean up all acids, bases, DI, Ta-wire-pieces, etc.

Edwards Auto 306 Evaporator Procedures

Sample preparation:

1. Degrease sample with solvents (acetone, methanol) DI rinse and N₂ blow dry.
2. Remove any oxides with 2 min of boiling aqua regia (HNO₃:HCl, 1:3), DI rinse and N₂ blow dry.

Vent chamber, Mount/Remove sample & Create vacuum:

1. Ensure chamber is not in use and has been cooled for at least ½ an hour after the last evaporation.
2. Press "**Seal/Vent**" and lift chamber clip—door will open *easily* at 7.6E2 Torr—not until!
3. When vented, **open** chamber door and remove sample jig—if removing, do so & go to Step 7.
4. **Mount** cleaned sample(s) properly on jig
5. Physically **verify** the metals in each carousel positions and note for assigning layer parameters.
6. Check amount of metal in hearths to be used and **fill only as necessary**—half full is OK.

7. **Insert jig** into chamber, and secure door.
8. Press “**Process**” to start vacuum.
9. **Fill** liquid N₂ reservoir to improve pump-down time.
10. Confirm metal **parameters** on each layer to be used (density, tooling, z-factor, etc.).
11. Program the **thickness** for each layer in nm.

Evaporation:

1. Wait until vacuum $\leq 2 \times 10^{-7}$ Torr is obtained.
2. Turn electron **Gun Power Supply ON**.
3. Turn **gun** and **on/off ON**, and wait for lights (Power, Vac, H₂O, Rot, Gun, Local, and Beam).
4. **Check** ~4.85 kV high voltage setting and 15-17 °C water chiller.
5. Using **Data** button, select appropriate layer and confirm settings changing as necessary.

	Ti	Al	Au	Ni
Layer	1	3	2	4
Density	4.5	2.7	19.3	8.91
Z-factor	14.1	8.2	23.2	26.6
Tooling	0.85	0.85	0.85	0.85
Beam for evap	120 mA	45 mA	100 mA	120 mA

6. Ensure shutter is **closed** and **no** shutter control buttons are pushed.
7. Activate **Beam Sweeping** by setting control knob to “1”.
8. Turn **Beam Current** control knob to 1st notch (~ 20 mA).
9. Slowly ramp **Beam Current** up in 20 mA steps every several seconds, monitoring vacuum pressure—don’t let pressure exceed 1×10^{-5} Torr.
10. If metal has not been used recently, **evaporate off impurities** by getting metal liquid hot (i.e., at the onset of evaporation—watch for solid to liquid phase change) otherwise go to step 12.
11. As necessary, allow chamber to return to 2×10^{-7} Torr, then repeat starting at step 9.
12. Stop ramping **Beam Current** when desired beam current is achieved, or turn down if 9×10^{-6} Torr is exceeded.
13. Arm shutter by depressing **Remote** button
14. Press “**Run**” to open shutter and start evaporation, noting start time.
15. Watch deposition rate and pressure; modify **Beam Current** to keep both within proper limits.
16. **Log** time when deposition completes.
17. Turn **Beam Current** down slowly (2-3 seconds) to zero.
18. Activate **Carousel** and move to position of next metal, else go to step 21 if done evaporating.
19. Using **Data** button, select appropriate layer and confirm settings changing as necessary.
20. Go to Evaporation step 8 when chamber returns to 2×10^{-7} Torr
21. Deactivate **Beam Sweeping**, **Carousel**, and disarm shutter **Remote**.
22. Turn **gun** and **on/off OFF**, turn **Gun Power Supply OFF**.
23. Log evaporation results into the Evaporation log book.
24. Wait at least ½ hour and follow vent procedures.

Bibliography

1. Fellows, James A. "Electrical Activation Studies of GaN implanted with Si from low to high dose", Appl. Phys. Lett., **80**:1930 (2002).
2. Pearton, S.J., et al. "GaN: Processing, defects, and devices", App. Phys. Rev., **86**:1 (1999).
3. S. Yoshida, S. Misawa, Gonda, J. Appl. Phys **53**:10 (1982)
4. Mohammad, Salvador, Markoc, Proceeding of the IEEE, **83**:10 (1995)
5. Fellows, James A. "Electrical Activation Studies of p-type Ion Implantation", Dissertation Proposal. Wright-Patterson AFB, OH: Air Force Institute of Technology (2000).
6. Bhattacharya, Semiconductor Optoelectronic Devices 2nd ed, New Jersey: Prentice Hall, 1997.
7. Judith L. McFall. "Optical Investigation of MBE $\text{Al}_x\text{Ga}_{1-x}\text{N}$ to Determine Material Quality", Wright-Patterson AFB, OH: Air Force Institute of Technology (2000)
8. "Ion Implantation And Metallic Contact Studies for Application to AlGaN Optoelectronic Devices", Dissertation Proposal. Wright-Patterson AFB, OH: Air Force Institute of Technology.
9. Fellows, James A. "Electrical Activation Studies of Ion Implanted Gallium Nitride", Wright-Patterson AFB, OH: Air Force Institute of Technology (2001).
10. McKelvey, Solid State Physics, Florida: Krieger Publishing Company, 1993.
11. Hong-Mei Wang, et al. "AlN/AlGa_N superlattices as dislocation filter for low-threading-dislocation thick AlGa_N layers on Sapphire", Appl. Phys. Lett., **81** (4) (2002).

12. J Blasing, et al., "The Origin of Stress reduced by low-temperature AlN interlayers", Appl. Phys. Let., **81**:15 (2002).
13. J.A. Bardwell, et al., "Comparison of two different Ti/Al/Ti/Au Ohmic metallization schemes for AlGaIn/GaN", J.Vac Sci. Technol., **20**:4 (2002)
14. Strite, S., et al. "GaN, AlN, and InN: A Review", J.Vac Sci. Technol., **10**: 1237 (1992).
15. Morkoc, H., et al. "Large-band-gap SiC, III-V nitride, and II-IV ZnSe-based semiconductor device technology", J. App. Phys., **76**:1363 (1994).
16. Ahoujja, M., et al. "Electrical and Optical investigation of MBE grown Si-doped AlGaIn as a function of aluminum mole fraction up to 0.5", Materials Science and Engineering, **B91-92**: 285 (2002).

Vita

Elizabeth Ann Chitwood was born in Colorado Springs, CO and moved to Ohio when she was four years old. She attended McAuley High School for girls in Cincinnati and was accepted to the University of Cincinnati, College of Arts and Sciences in the fall of 1996. After completion of the physics program she was awarded a Bachelor of Science degree in Physics and a minor in Mathematics. Her academic studies then took her to Dayton, OH where she attends the Air Force Institute of Technology. She is on a DAGSI scholarship and is currently working towards a PhD in Physics.

REPORT DOCUMENTATION PAGE

Form Approved
OMB No. 074-0188

The public reporting burden for this collection of information is estimated to average 1 hour per response, including the time for reviewing instructions, searching existing data sources, gathering and maintaining the data needed, and completing and reviewing the collection of information. Send comments regarding this burden estimate or any other aspect of the collection of information, including suggestions for reducing this burden to Department of Defense, Washington Headquarters Services, Directorate for Information Operations and Reports (0704-0188), 1215 Jefferson Davis Highway, Suite 1204, Arlington, VA 22202-4302. Respondents should be aware that notwithstanding any other provision of law, no person shall be subject to a penalty for failing to comply with a collection of information if it does not display a currently valid OMB control number.

PLEASE DO NOT RETURN YOUR FORM TO THE ABOVE ADDRESS.

1. REPORT DATE (DD-MM-YYYY) 03-10-2002		2. REPORT TYPE Thesis		3. DATES COVERED (From – To) Jan 2003 – March 2003	
4. TITLE AND SUBTITLE ELECTRICAL ACTIVATION STUDIES OF SILICON IMPLANTED $\text{Al}_x\text{Ga}_{1-x}\text{N}$ AND COIMPLANTED GaN				5a. CONTRACT NUMBER	
				5b. GRANT NUMBER	
				5c. PROGRAM ELEMENT NUMBER	
6. AUTHOR(S) Elizabeth A. Chitwood				5d. PROJECT NUMBER	
				5e. TASK NUMBER	
				5f. WORK UNIT NUMBER	
7. PERFORMING ORGANIZATION NAME(S) AND ADDRESS(ES) Air Force Institute of Technology Graduate School of Engineering and Management (AFIT/EN) 2950 P Street, Building 640 WPAFB OH 45433-7765				8. PERFORMING ORGANIZATION REPORT NUMBER AFIT/GAP/ENP/03-01	
9. SPONSORING/MONITORING AGENCY NAME(S) AND ADDRESS(ES) Air Force Office of Scientific Research 4015 Wilson Blvd. Arlington, VA 22203				10. SPONSOR/MONITOR'S ACRONYM(S) AFOSR/NE	
				11. SPONSOR/MONITOR'S REPORT NUMBER(S)	
12. DISTRIBUTION/AVAILABILITY STATEMENT APPROVED FOR PUBLIC RELEASE; DISTRIBUTION UNLIMITED.					
13. SUPPLEMENTARY NOTES					
14. ABSTRACT <p>A comprehensive study of the electrical activation of silicon implanted $\text{Al}_x\text{Ga}_{1-x}\text{N}$ was performed as a function ion dose, anneal temperature, and aluminum mole fraction. Also, GaN coimplanted with silicon and nitrogen was investigated. Room temperature Hall effect measurements were used to determine carrier concentration and mobility. All the samples had a 500 Å encapsulant of AlN, and were implanted at room temperature with 200 keV silicon ions at doses ranging from 1×10^{13} to $1 \times 10^{15} \text{ cm}^{-2}$. The GaN was also implanted with nitrogen under the same conditions in doses of 9×10^{12} to $9 \times 10^{14} \text{ cm}^{-2}$, respectively. The samples were annealed at temperatures ranging from 1200 to 1350 °C for 30 to 120 seconds in a flowing nitrogen environment. The aluminum mole fractions considered were 0.2 and 0.3. The electrical activation efficiency for the $\text{Al}_{0.2}\text{Ga}_{0.8}\text{N}$ annealed at 1350 °C and implanted with $1 \times 10^{15} \text{ cm}^{-2}$ was almost 90%. While the $\text{Al}_{0.3}\text{Ga}_{0.7}\text{N}$ annealed at 1350 °C and implanted with $1 \times 10^{15} \text{ cm}^{-2}$ exhibited only about 42% activation. Although the $\text{Al}_{0.2}\text{Ga}_{0.8}\text{N}$ exhibited almost perfect activation, the mobility was generally low, only $50 \text{ cm}^2/\text{V}\cdot\text{s}$. The coimplanted GaN showed surprisingly poor results. The highest activation efficiency was only 37% for the sample annealed at 1300 °C and implanted with a dose of 1×10^{15} silicon ions cm^{-2}. The mobilities for these samples were high, on average $100 \text{ cm}^2/\text{V}\cdot\text{s}$.</p>					
15. SUBJECT TERMS Electrical activation efficiency, GaN, AlGaIn, Hall effect, Implantation					
16. SECURITY CLASSIFICATION OF:			17. LIMITATION OF ABSTRACT UU	18. NUMBER OF PAGES 75	19a. NAME OF RESPONSIBLE PERSON Dr. Yung Kee Yeo, ENP
a. REPORT U	b. ABSTRACT U	c. THIS PAGE U			19b. TELEPHONE NUMBER (Include area code) (937) 255-3636, ext 5432

